NASA Contractor Report 166066

NASA-CR-166066
19830010911

Study and Simulation Results for Video Landmark Acquisition and Tracking Technology (VILAT-II)

J. W. Lowrie, J. C. Tietz, H. M. Thomas,
K. D. Gremban, C. Hughes, and C. Y. Chang

MARTIN MARIETTA AEROSPACE
Denver Aerospace
Denver, Colorado 80201

Contract NAS1-15602
February 1983

National Aeronautics and
Space Administration

Langley Research Center
Hampton, Virginia 23665

FOREWORD

This document covers the work performed under Contract NAS1-15602, Study and Simulation Results for Video Landmark Acquisition and Tracking Technology (VILAT-II), for the Langley Research Center of the National Aeronautics and Space Administration. It was prepared by Martin Marietta Corporation in accordance with the contract Statement of Work.

Use of commercial products or names of manufacturers in this report does not constitute official endorsement of such products or manufacturers, either expressed or implied, by the National Aeronautics and Space Administration.

This Page Intentionally Left Blank

CONTENTS

FIGURES

TABLES

CHAPTER I - INTRODUCTION

Examination of advanced NASA mission models (Ref. 1) reveals that future remote-sensing missions will require increasingly complex subsystems and support procedures. One measurement of this trend is the resolution of the onboard science sensor, because this figure directly affects the onboard data rates and the required navigation accuracy. Landsat D, which was scheduled for launch in July of 1982, will have a spatial resolution of 30 meters (if the thematic mapper is incorporated), and the Advanced Land Observing System (ALOS), which will be implemented in 1989, will acquire imagery in 20 different bands with a 15-meter resolution. Whereas one scene of imagery currently constitutes 3×10^8 bits of data, in 1985 the same scene acquired in the additional bands with higher resolution will constitute 2×10^{10} bits—an increase of two orders of magnitude in just five years! In addition to affecting the data rates, increased resolution impacts the following areas:

- Greater processing requirements for image correction;
- Increased navigation accuracy to provide useful distortion coefficients;
- Increased archiving requirements.

To compound the problem, user communities are generally requiring data in shorter periods of time. Currently, Landsat turnaround time is measured in weeks and can be as much as two months. Users of future remote-sensing imagery require this time to be cut to hours. To overcome the limitations associated with existing remote-sensing missions, revolutionary approaches are required in the next generation of spacecraft.

As a prerequisite of plotting a course toward the design of future remote-sensing spacecraft, it is imperative that the interrelationships between subsystems, operational support, and user requirements be identified. A knowledge of these interrelationships will allow new approaches and their inherent impact on the overall system to be fully understood.

Figure I-1 illustrates the current state of remote-sensing missions. By 1985 these missions will acquire in excess of 10^{15} bits of data per day or roughly equivalent to 30 libraries of congress a year (Ref. 2). The acquisition of these data is totally nondeterministic in that nothing is known about the quality, content, or location of the imagery prior to or even shortly after it is obtained. As a result, very little of the data is used by the scientific community because of undesirable effects such as cloud coverage, unwanted scene content, or exposure dates that do not coincide with those desired. In fact, less than 1% of all previously acquired remotely sensed data has been examined by users.

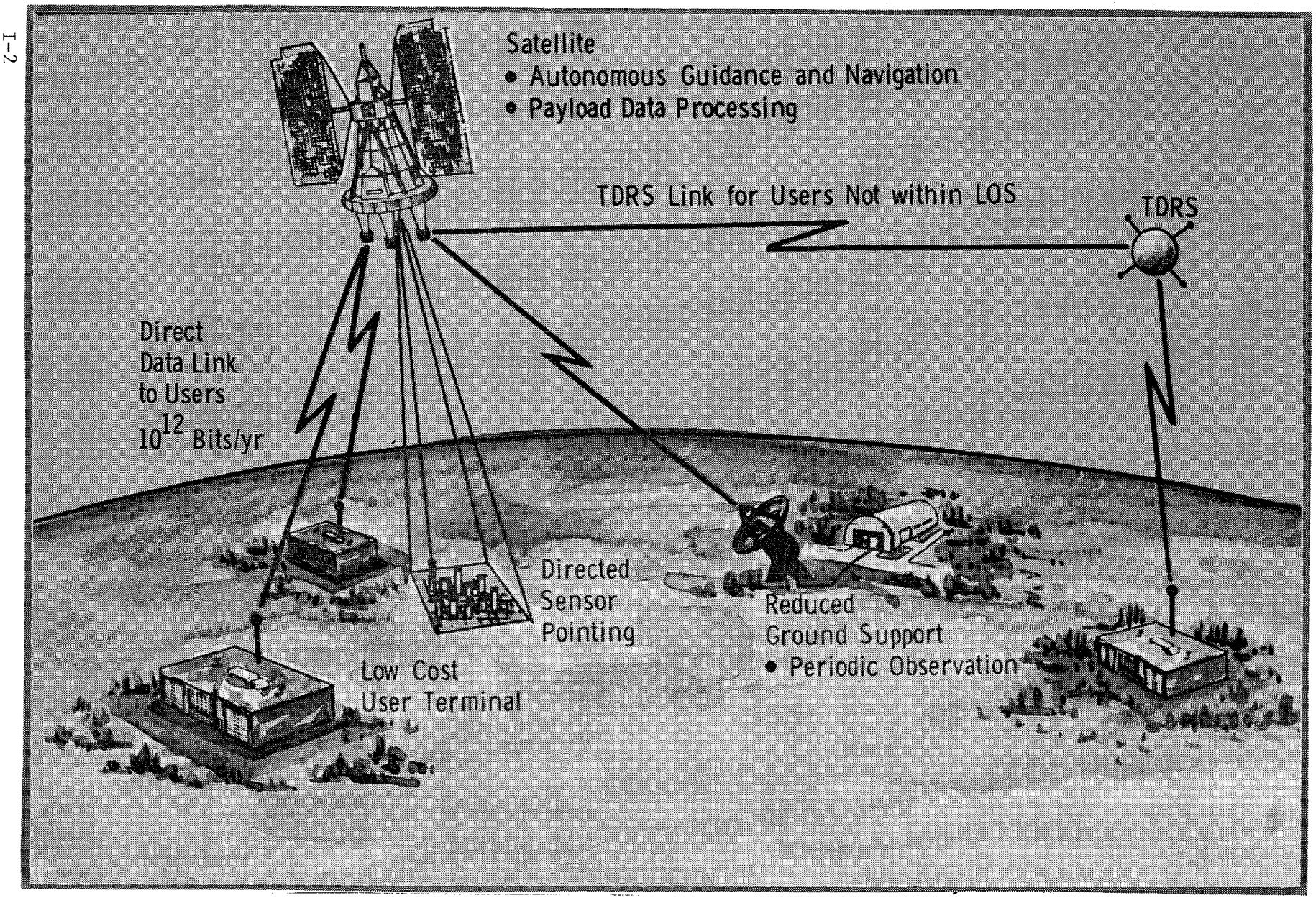

Figure I-1 The State of Current Remote-Sensing Missions

In addition to the data deluge problem, it is currently not feasible to exploit Landsat data for real-time applications such as forest fire detection and monitoring and flood detection. In fact, with the exception of applications where the observables do not change dramatically with time (such as oil exploration), Landsat is of little value from an operational standpoint because the data are already stale by the time the user gets them. In examining the problem more closely, it becomes apparent that the following areas are the most critical items:

- Remote-sensing systems do not employ any techniques of data evaluation for either negation or simple annotation. A simple determination of the percentage of clouds in a scene could be used to eliminate about 50% of all data acquired. To be most effective, data evaluation should be performed at the sensor so no delays lead to a bottleneck and so data negation, which promises to be a powerful technique, can be implemented;

- Users are subject to the mission schedule rather than the mission being tailored to the specific acquisition requirements of the user. As a result, many users must settle for nonoptimal viewing conditions;

- All data, including tracking information from remote stations, are sent to a central facility for image correction, annotation, and packetization and are then sent to another remote facility for archiving and eventual dissemination to the users. The process is neither cost- nor time-effective and results in an unmanageable data base;

- No advantage is being taken of the onboard navigation capability for control of the spacecraft to limit the image distortion or to enable selective acquisition through sensor pointing.

The objective of the Video Landmark Acquisition and Tracking (VILAT) contract was to identify and investigate dramatically new approaches to remote sensing to meet the goals of future missions. An example of the remote-sensing techniques being investigated under the VILAT contract is illustrated in Figure I-2. The representative satellite illustrated possesses several key features that make it attractive for remote-sensing missions. Deterministic data acquisition to meet specific user requirements may be realized through onboard classification, tracking of features, and controlled pointing to predefined coordinates. Autonomous image correction is provided through increased control of the spacecraft and special design of the science instrument. Real-time detection of certain critical events such as forest fires is provided, and the flow of data is tailored to user requirements. Through automated archiving techniques, near-real-time dissemination is provided to users who are not hindered by time-varying observables. Several spinoffs make this approach particularly attractive. Onboard image correction and directed sensor pointing require onboard navigation and control, thus reducing the amount of ground support for that particular mission. Furthermore, reduced data rates may be achieved even in the presence of higher resolution sensors through data-set selection, information extraction, and modest data compression.

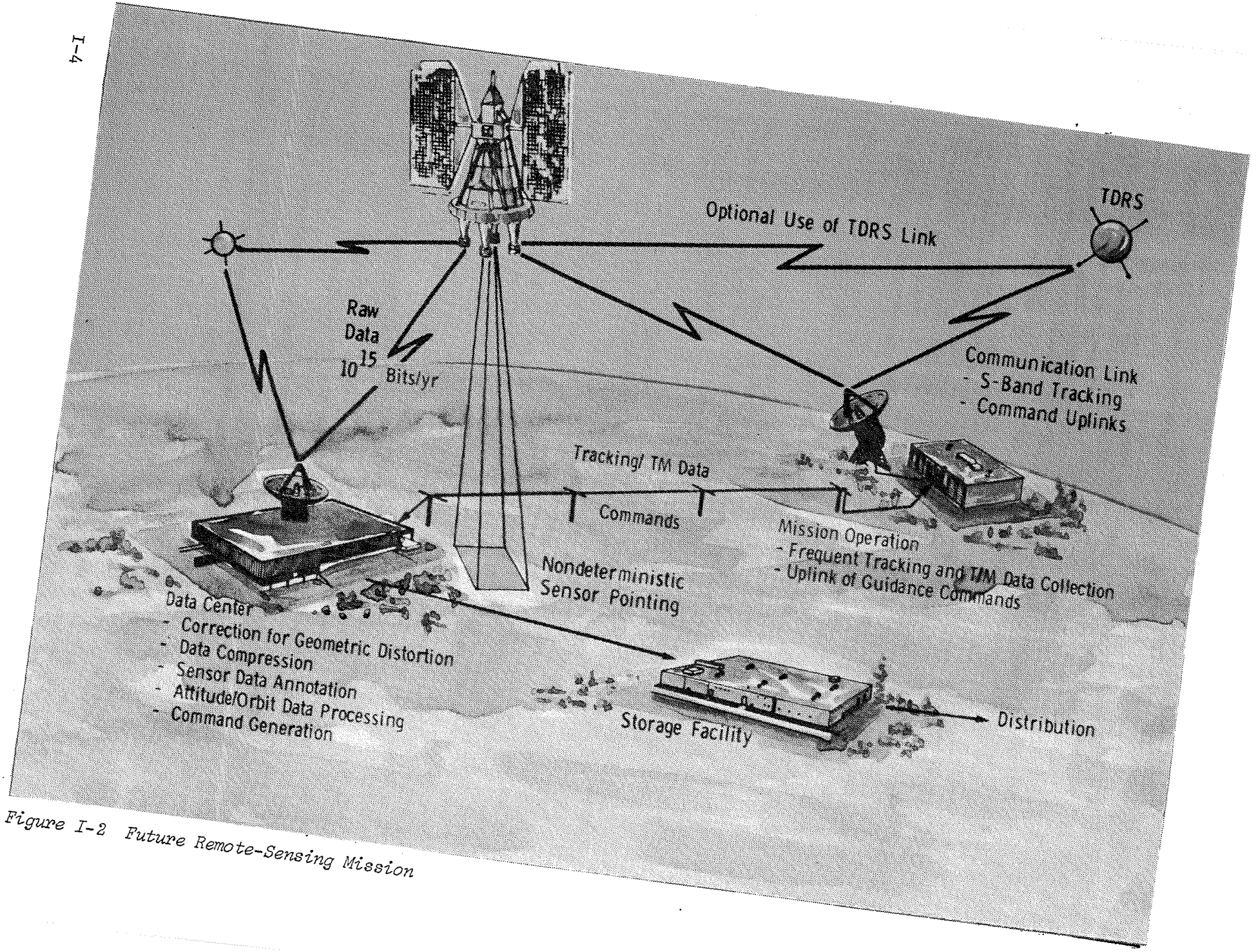

Figure I-2 Future Remote-Sensing Mission

The approach to developing concepts for future remote-sensing missions has been systematic to ensure a steady, well-planned advancement of the state of the art toward the goal of real-time remote-sensing applications. The role of VILAT has been to develop and analyze concepts for eventual experimental flight testing under the Feature Identification and Location Experiments (FILE) contract (Ref 3).

This development effort began in 1976 with the conception and analysis of multispectral ratio techniques for real-time classification of imagery (Ref 4). The concept is based on the principle that certain classes of features can be separated according to their spectral signature alone and that a ratio of sensor outputs taken in two specific spectral bands not only separates these features but is relatively insensitive to atmospheric variations and light level. It is intended that, for a given application, the outputs from such a sensor system would be used to either annotate the imagery or to selectively negate data acquisition during periods when the primary observable is not present.

Classification is performed on a picture-element basis by using the spectral signature. Field measurements confirmed that the four feature types--vegetation, bare land, water, and clouds or snow--can be separated by radiance measurements at two discrete wavelengths, 650 and 850 nm. The former wavelength corresponds to the chlorophyll absorption band where healthy green vegetation has very low reflectance. The 850-nm band is in the near-infrared where healthy green vegetation has high reflectance, as do clouds, snow, and bare land, whereas water has extremely low reflectance, as shown in Figure I-3.

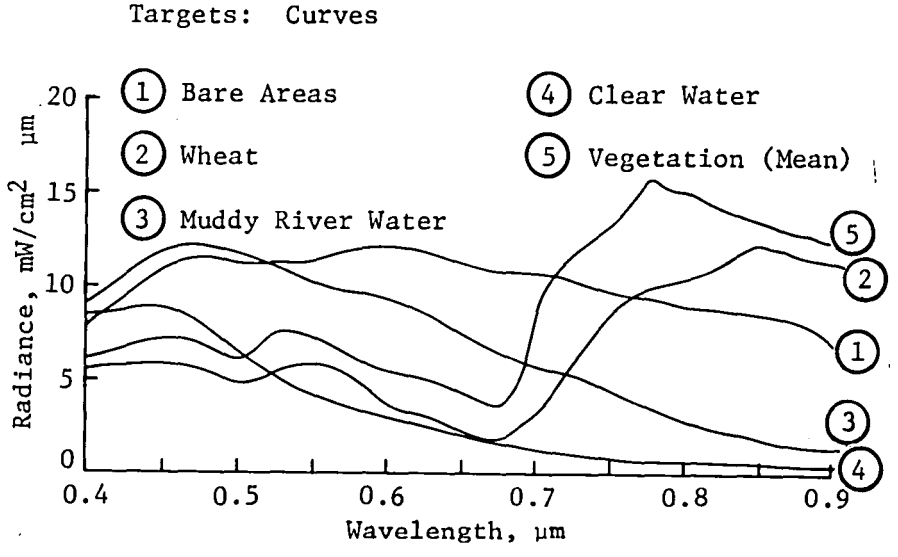

Figure I-3 Target Spectral Radiances

The observed radiance from an object is a function of its reflectance and the radiance and absorption characteristics of the medium through which it is viewed. However, the ratio of the radiances at two wave-lengths is relatively independent of such parameters as look angle and atmospheric effects. The FILE-I experiment separates water, vegetation, and clouds/snow/bare earth on the basis of a ratio between the 650 and 850 nm bands. Bare earth and clouds/snow can be further separated on the basis of absolute radiance in the 650 nm band. This can be done with approximation of the solar illumination angle because clouds and snow have a higher reflectance than most types of bare land. Figure I-4 illustrates how the various features are separated with the multispectral classification algorithm.

In addition to the multispectral ratio technique, VILAT also investigated the concept of deterministic acquisition through sensor pointing. The original algorithm was developed for specific applications such as water pollution monitoring and estuary research where the primary data of interest were the land/water interfaces. The algorithm developed computed inputs to a pointing mount so the boresight remained centered on the land/water interface to eliminate all other nonessential data.

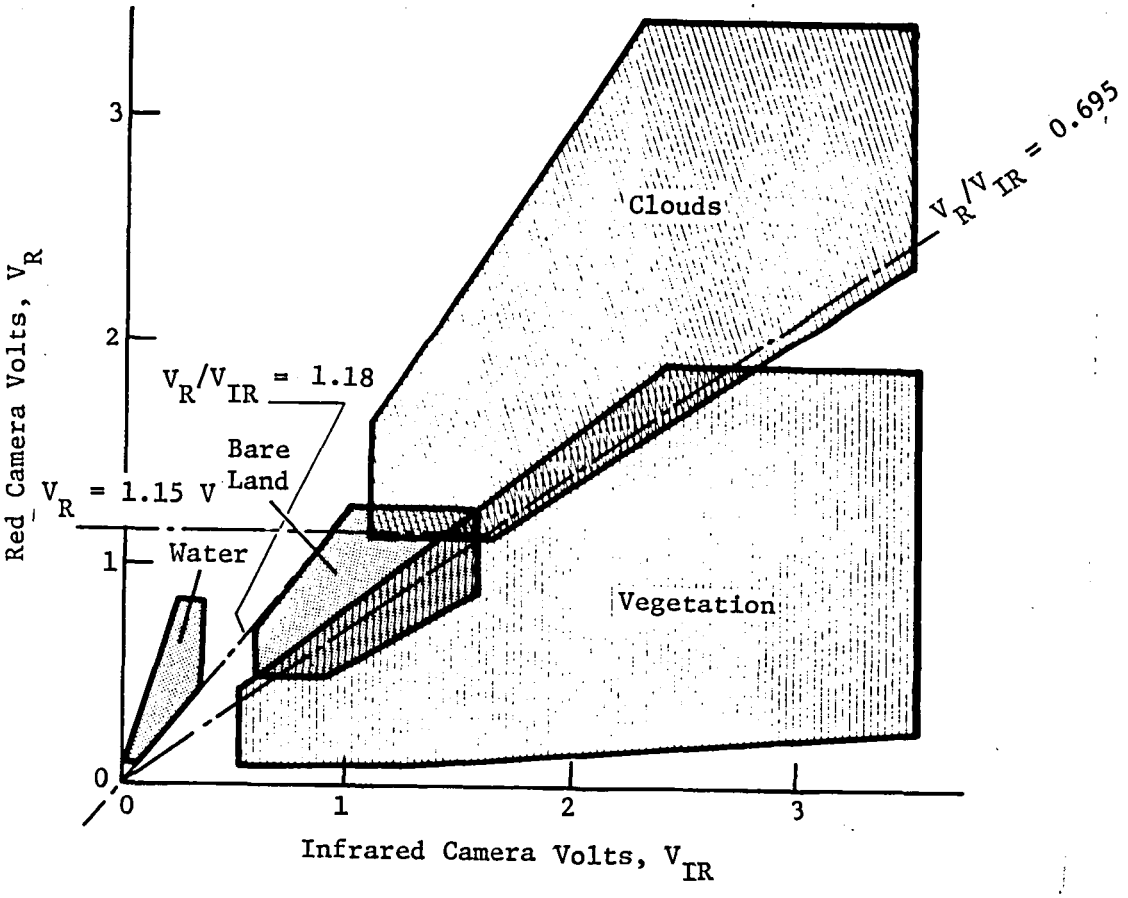

Figure I-4 99% Confidence Polygons for Feature Classification

The VILAT algorithms developed have been based on the principle that a future remote-sensing platform could have a number of selective acquisition techniques for each application and that these algorithms could be implemented when users requested data, suggesting the evolution of a truly adaptive remote-sensing system.

The specific objectives for the latest VILAT contract were in the following areas:

- Expand the multispectral ratio technique to allow additional classification of snow and ice. This development is a significant step toward an operational cloud detector for a wide class of missions;

- Survey the state of the art of IR detectors for incorporation in the FILE-II cloud detector experiment;

- Construct an IR radiometer from an appropriate IR detector to verify the cloud/snow/ice discriminator;

- Obtain field test data with the IR radiometer;

- Construct a signal processor to form the heart of future experiments;

- Construct a second ground support equipment (GSE) unit so that aircraft flight tests could be conducted while FILE-I was awaiting Shuttle launch;

- Define FILE-II, which will be capable of discriminating between vegetation, bare earth, water, clouds, snow, and ice;

- Develop a comprehensive set of data analysis tools to allow meaningful analysis of data obtained from the Shuttle and aircraft flight tests of FILE-I;

This report thoroughly describes the concepts, analysis procedures, and results developed under the VILAT contract and has been separated into six chapters entitled:

I - Introduction;

II - Multispectral Ratioing Techniques for Remote Sensing;

III - IR Camera Definition;

IV - VILAT Processor and Ground Support Equipment

V - FILE-II Preliminary Definition;

VI - Data Analysis Procedures;

REFERENCES

1. Lowrie, J. W., "Autonomous Navigation Systems Technology Assessment", AIAA Paper No. 79-0056, 17th Aerospace Sciences Meeting, New Orleans, La., January 15, 1979.

2. A Forecast of Space Technology: 1980-2000. National Aeronautics and Space Administration Office of Scientific and Technical Information, NASA SP-387, January 1976.

3. R. Gale Wilson and W. Eugene Sivertson, Jr. "Earth Feature Identification and Tracking Technology Development," Paper presented at Society of Photo-Optical Instrumentation Engineers, Technical Symposium East, Washington, DC, April 17-20, 1979.

4. R. T. Schappell, J. C. Tietz, H. M. Thomas, and J. W. Lowrie. Experimental and Simulation Study Results for Video Landmark Acquisition and Tracking Technology. Martin Marietta Denver Aerospace NASA Contractor Report 158997, February 1979.

CHAPTER II MULTISPECTRAL RATIOING TECHNIQUES FOR REMOTE SENSING

A. OVERVIEW

It has become increasingly popular to use the spectral ratios of satellite collected imagery for processing agricultural data and for mapping mineralogically important areas (Ref. 1-3). The rationales behind these ratio techniques are that they minimize the influence of topography and overall albedo on the grouping of spectrally similar materials, and that the spectral ratios tend to compensate for some of the multiplicative factors such as the haze and atmospheric effects on the multispectral data.

The intent of this study was to identify the capabilities and limitations of multispectral ratio classification. In particular the primary goal of this task was to show that the separation of clouds from snow and ice is feasible. FILE-I already separates water, bare land, and vegetation from clouds/snow/ice and with this additional classification capability FILE could become an operational cloud detection system capable of autonomous data selection. Also of interest is the separation of fresh snow coverage from ice. With this capability FILE could be used on missions, such as ICEX, for automated mapping of the ice fields and glaciers present in the world. The FILE classification algorithm was never intended to provide general classification of detailed feature types, as LACIE is, but it is important to understand the full capabilities and limitations of the technique. This chapter addresses these issues.

A number of interesting results from ratio techniques have been reported in various literatures. Limitations of the techniques have also been discussed. In most cases, the spectral bands chosen are based on the characteristic reflectance spectra of categories of interest. Taking green vegetation as an example, the spectral reflectances for vegetation and soil as shown in Figure II-1 suggest that the red (0.63 - 0.69 μm radiance) to near-infrared spectral ratio provides the greatest discrimination between green vegetation and soil. On the other hand, the pronounced effect of vegetation cover on various rock types over the spectral range of 0.7 to 1.3 μm strongly implies that the spectral bands outside of this range should be used to effectively discriminate among different rock and soil types (Ref. 4 and Fig. II-2). In either case, however, the spectral ratio consistently shows improved discriminatory power over the individual spectral bands taken separately.

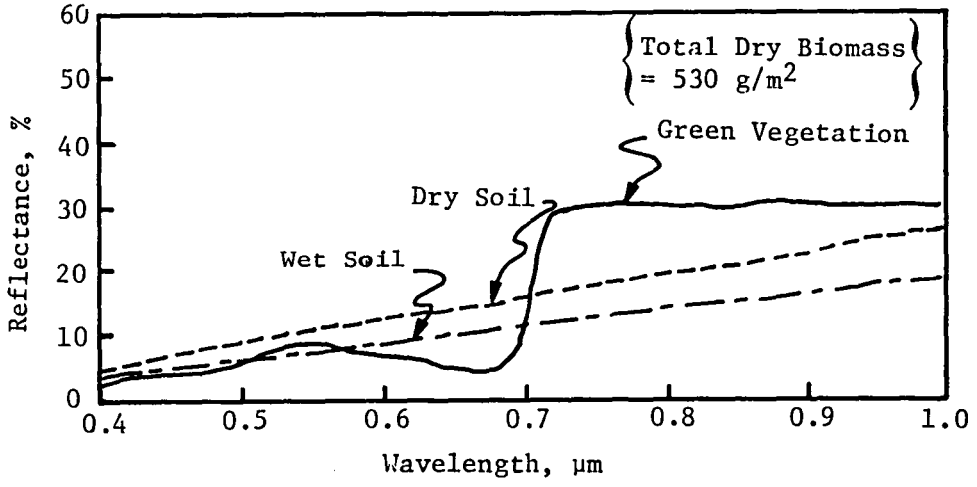

Figure II-1 Spectral Reflectances for Dry Soil and Green Vegetation (After Fig. 2 of Ref. 2)

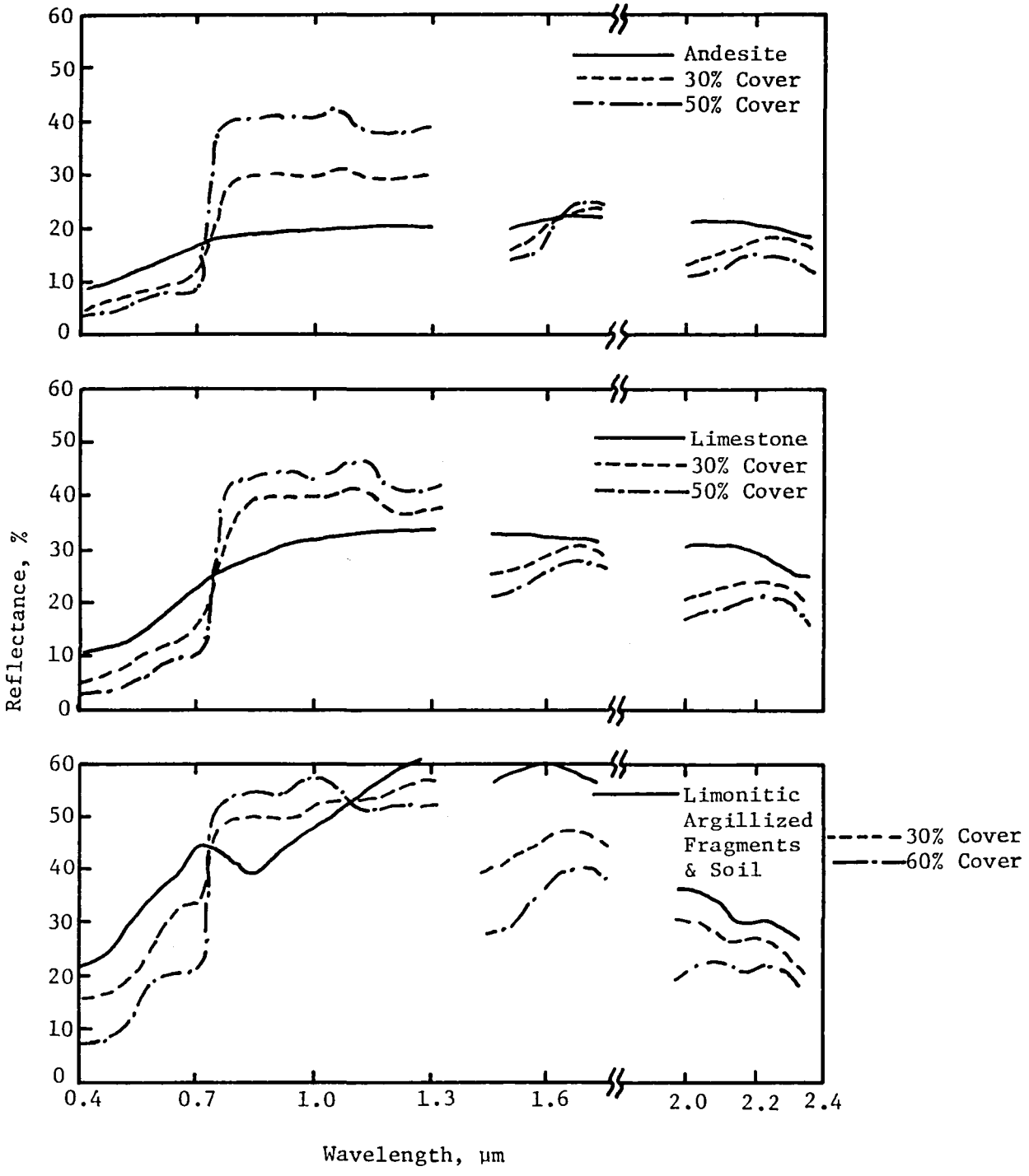

Figure II-2 Effect of Varying Amount of Green Grass

B. CHARACTERISTIC REFLECTANCE SPECTRA

An examination of various reflectance spectra will often provide insight into the relationship between the spectral bands and various categories of interest. In the following paragraphs the spectral signatures of the primary targets of interest (i.e., water, bare earth, vegetation, clouds, snow, and ice) are discussed.

VEGETATION

Figure II-1 has already depicted the difference in the spectral reflectances between the typical green vegetation with total dry biomass of 530 g/m^2 and two types of soil. As expected, the moisture content of the leaves has strong influence on the leaf reflectance (Figure II-3). The so-called water absorption bands are particularly evident at approximately 1.45 and 1.95 μm. In general, marked increases in reflectance are observed with decreasing moisture content throughout the 0.5 - 2.6 μm region. For dry leaves, the lacking chlorophyll leads to the absence of the cholorphyll absorption band at approximately 0.66 μm, thus giving the leaf its brilliant red coloration, so familiar in the fall season. As a result of this phenomenon, it is expected that the percentage misclassification of vegetation will increase during drought conditions and in late fall and winter.

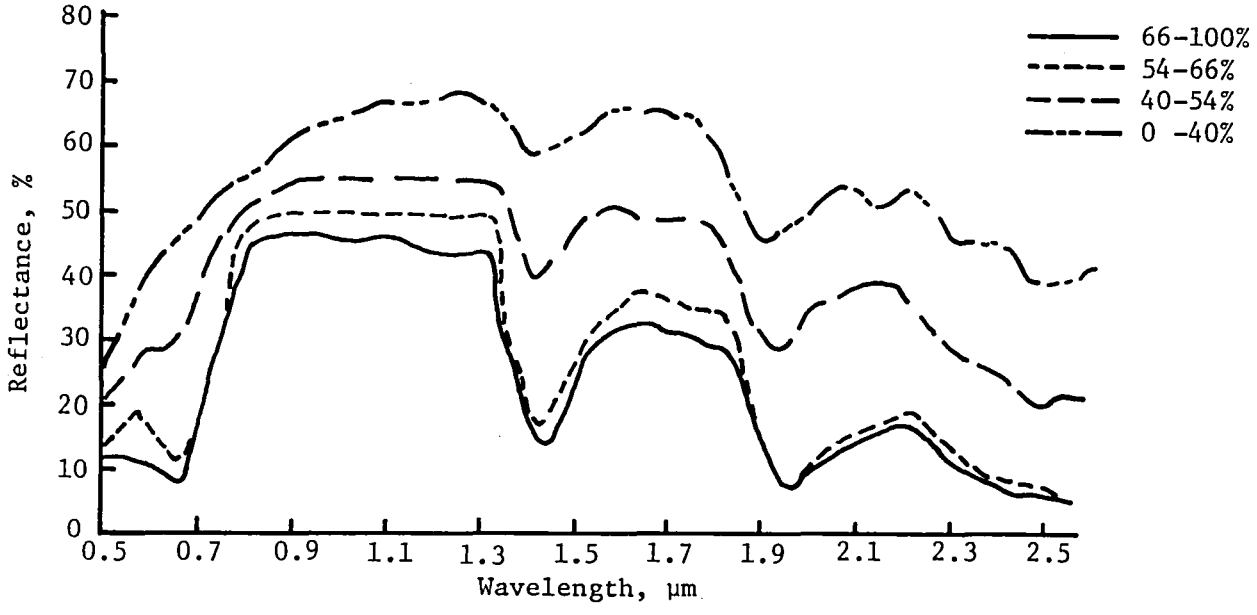

Figure II-3 Effects of Moisture Content on Corn Leaf Reflectance Spectra (Ref. 5)

BARE EARTH

The spectral reflectance signature of bare earth varies with type but can generally be described by a slowly increasing function of wavelength between .4 and 1.3 μm. However, the effect of moisture content on various soil types is pronounced. Figure II-4 shows in-situ spectral reflectance of two soil types at different moisture levels. It is noted that the curves for both soil types exhibit a large increase in reflectance with decreasing moisture content. The water absorption bands at the neighborhood of 1.45 μm and 1.95 μm become pronounced for sandy soils with a moisture content of over 4% and for clay soils of any moisture levels. At any rate, the wet soils appear to be much less reflective than green vegetation in the near IR region between 0.72 and 1.3 μm. Moreover, the red cholorophyll absorption band of about 0.66 μm is conspicuously missing in most soil reflectance curves. On the basis of this discussion, it is expected that the primary misclassification of bare earth will be caused by high moisture content. One exception to this, however, is limonitic-type soils where the absolute reflectance approaches that of clouds.

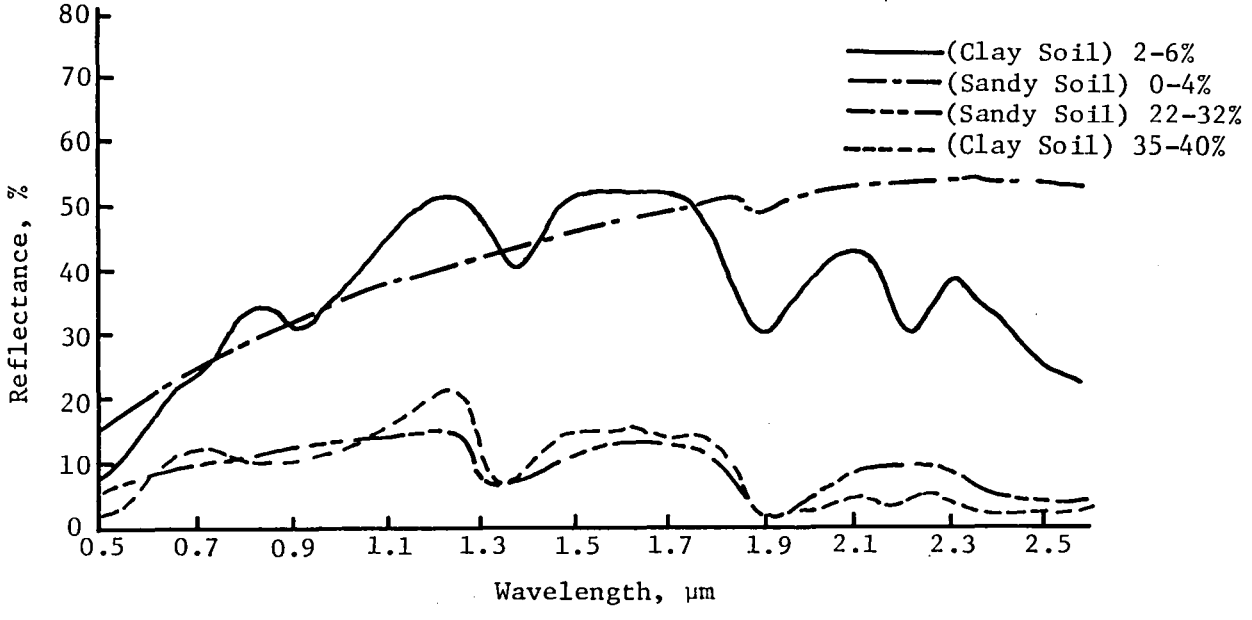

Figure II-4 Effects of Moisture Content on Two Soil Types Reflectance Spectra (Ref. 5)

WATER

The water spectral reflectance is a complex function of solar elevation angles, sediment constituents and concentration, and water surface and bottom conditions. For clear fresh water and sea water, the reflectance curve peaks at approximately 0.42 μm. But when the water is contaminated with either inorganic sediments or organisms like phytoplankton, the peak of the reflectance tends to shift toward the red spectrum of 0.52 - 0.58 μm as illustrated in Figure II-5. It seems from this figure that the 0.52 - 0.58 μm range is effective for detection of underwater features and assessment of sediment concentrations. Beyond 0.75 μm, the water completely absorbs the near IR wavelengths. Since the vegetation and soils generally exhibit high reflectance in the near IR region, it suggests that the 0.75 - 1.1 μm spectral range can be very effective in delineation of the land-water boundary. Furthermore, it is expected that very little misclassification of water will occur except in the presence of very high sediment content.

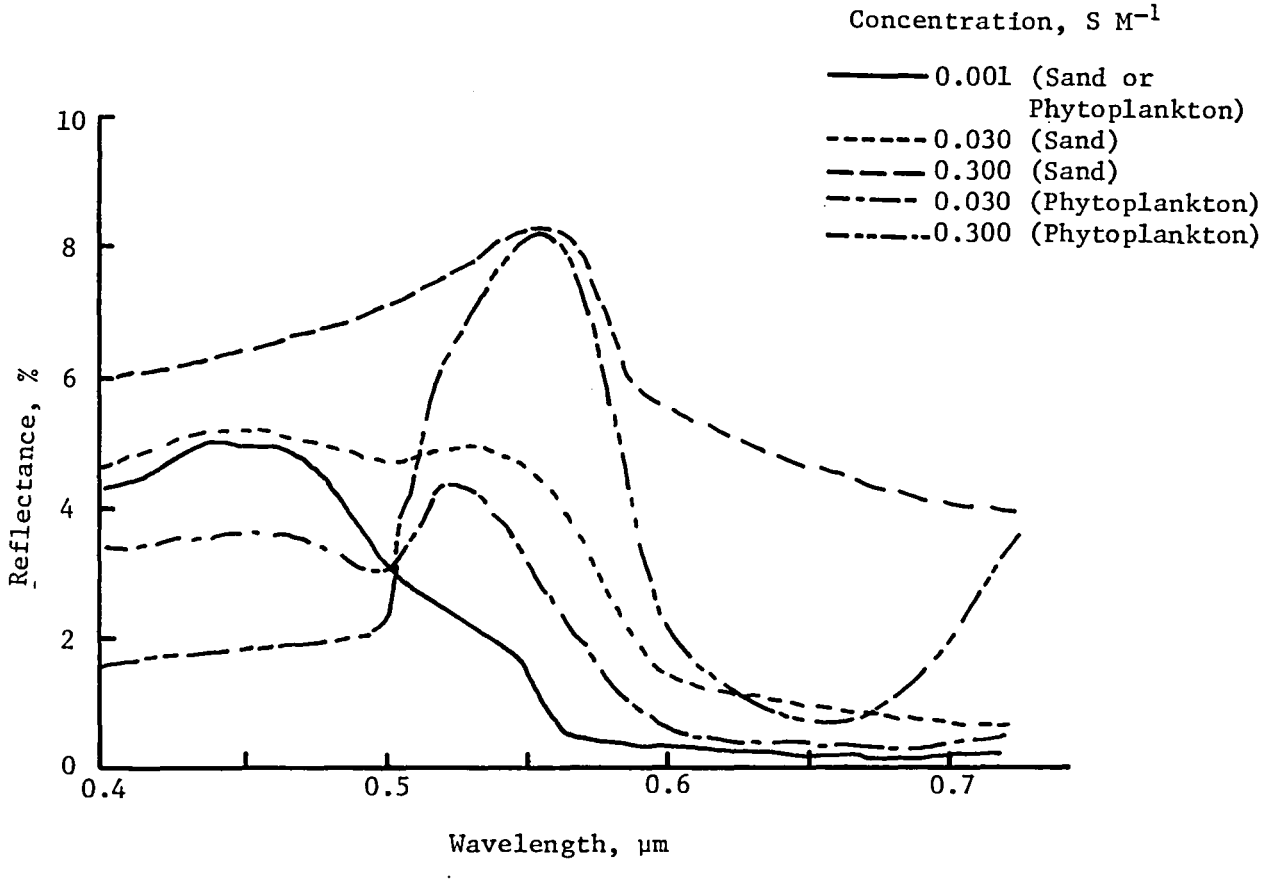

Figure II-5 Effects of Sediments and Organisms on Water Reflectance Spectra (Ref. 6)

SNOW

Snow, one of the important water resources to be observed from space, exhibits quite a different reflectance characteristic from other categories (see Fig. II-6 and II-7). It is highly reflective from the entire visible spectrum through the near IR to at least 1.4 μm. But from about 1.5 μm to 3.0 μm, the snow becomes highly absorbent, appearing almost non-reflective. This observation coincides with the findings in Reference 9 based on Skylab imagery studies. It is reported that in the visible band S192 imagery, snow has very high reflectance. In the Bands 11 and 12 imagery (spectral ranges of 1.55 - 1.75 μm and 2.10 - 2.35 μm, respectively) however, the snow is essentially non-reflective. Figure II-7 tends to substantiate the aforementioned conclusions. Therefore, the 1.55 - 1.75 μm and 2.10 - 2.35 μm spectral bands would be of great use in isolating snow and ice from other features.

An additional study was performed to determine the feasibility of separating snow from ice. From Reference 8 and Figure II-7 the reflectance of snow in the region of 1.0 to 1.4 μm changes as a function of density. Based on this observation it may be possible to separate ice from fresh snow using a narrow band measurement centered around 1.2 μm. However, the variables affecting this decision process and even the phenomenon itself are not well defined or analyzed. For example, in a paper by J. C. Barnes and M. D. Smallwood, "Snow Survey from Space, with Emphasis on the Results of the Analysis of Skylab EREP S192 Multispectral Scanner Data," (Ref. 9) some phenomena were attributed to surface snow melting causing a surface layer of water. The paper further states that if the melting snow were to refreeze, the reflectance would be the same as dry or new snow. Both references do support the differentiation between clouds and snow in the 1.55 - 1.75 μm spectral band. The unavailability of conclusive data in the 1.2 - 1.4 μm spectral band suggests further study be done by obtaining a sensor in this range and gathering data on snow and ice in various stages of development.

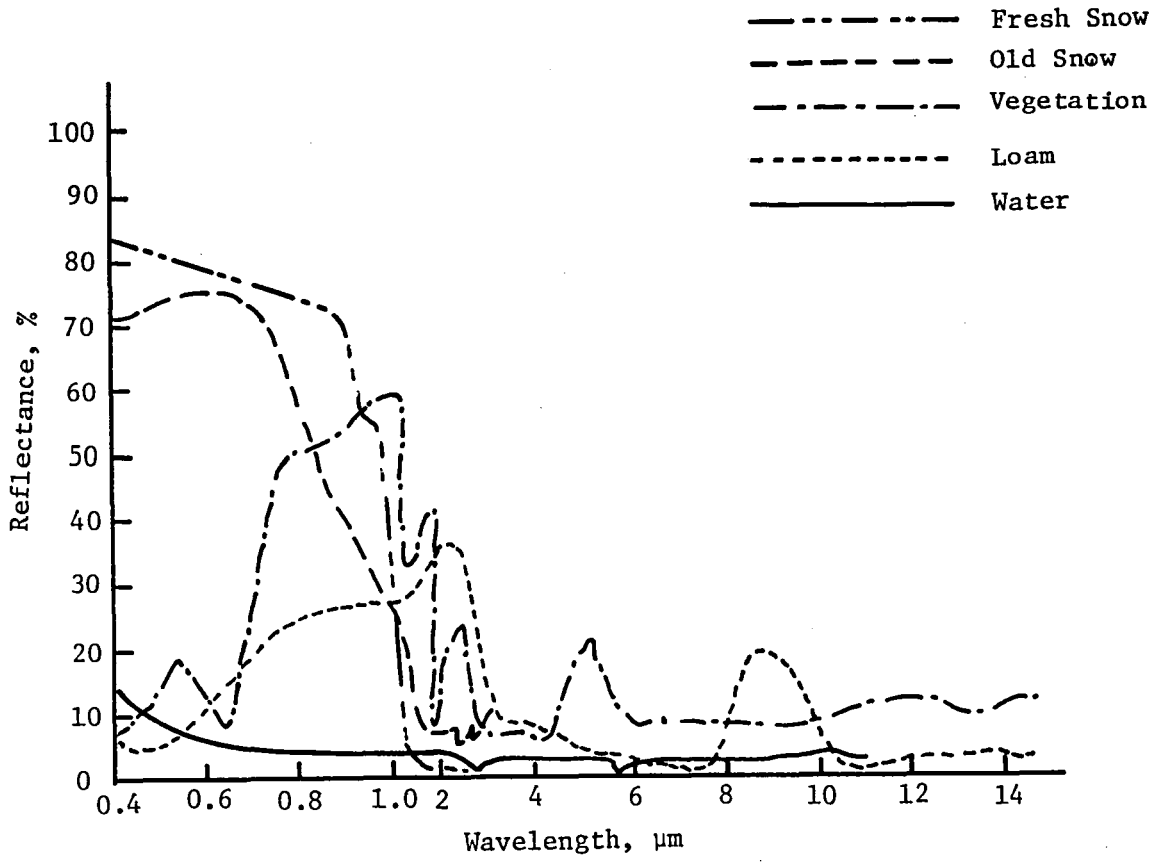

Figure II-6 Typical Reflectance Spectra for Snow, Water, Loam, and Vegetation (Ref. 7)

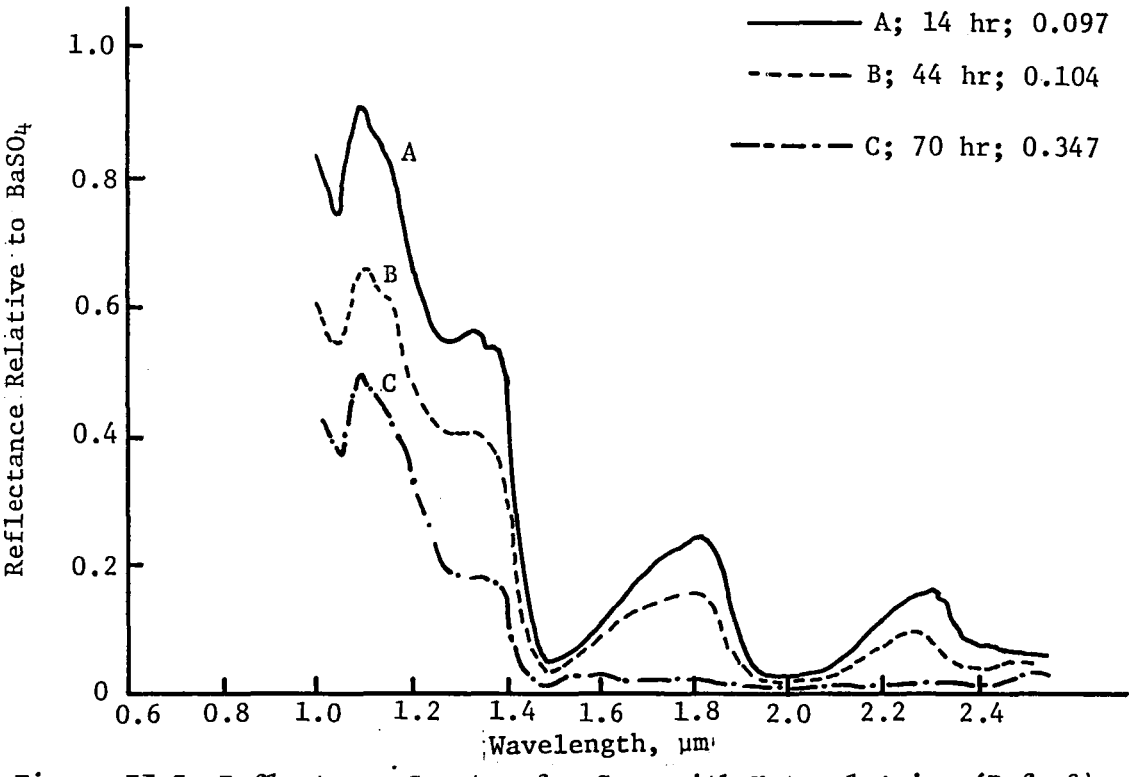

Figure II-7 Reflectance Spectra for Snow with Natural Aging (Ref. 8)

CLOUDS

Clouds typically exhibit very high reflectance across the spectrum between .4 and 1.8 μm. However, past 1.8 μm the water absorption bands become predominant (Fig. II-8). From an analysis of spectral signatures clouds may be separated from vegetation, bare earth, and water according to percentage reflectance in a narrow band centered at .65 μm. However, to further discriminate clouds from snow and ice it is necessary to perform a thresholding on the basis of reflectance in a band centered at 1.55 μm where clouds typically have high reflectance while snow and ice are almost totally absorbent. It is observed that the reflectance of clouds varies somewhat as a function of density, but it is not anticipated that this will produce any misclassification.

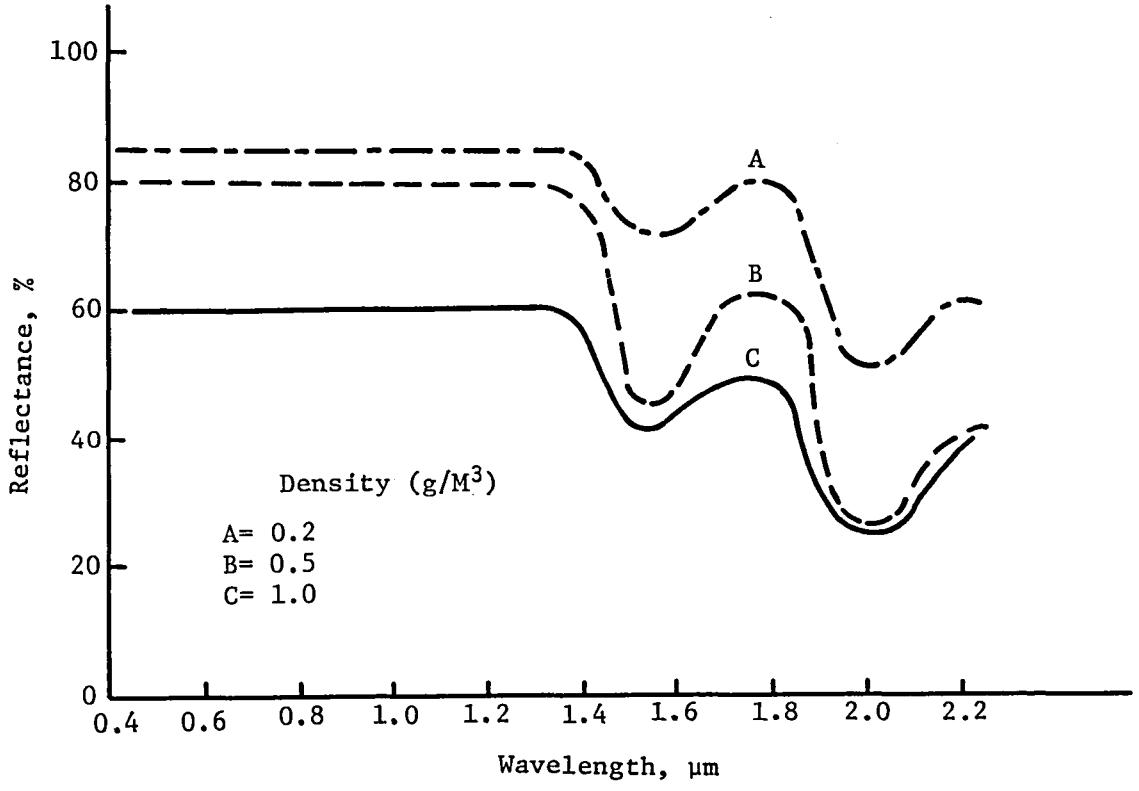

Figure II-8 Cloud Spectral Reflectance (Ref. 10)

C. ATMOSPHERIC CONSIDERATIONS

As a useful guideline in selecting spectral bands for use in the satellite sensor system, the band should always fall into an atmospheric "window." Figure II-9 depicts the atmospheric transmission characteristics that must be considered when selecting the proper bands. It is interesting to note that the only thermal IR band used in the Skylab EREP multi-spectral scanner (10.2 to 12.5 μm) is also in a "window." For classificational purpose, it has been reported (e.g. Ref. 12) that this thermal band is relatively effective for agricultural data processing.

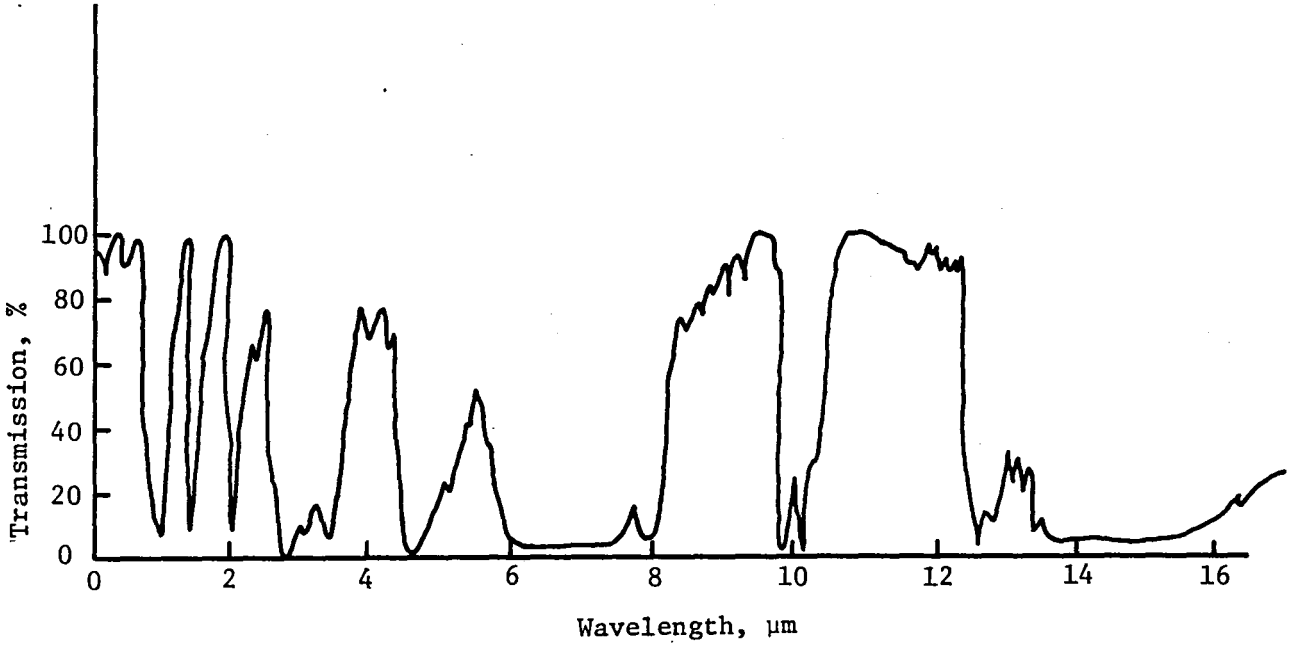

Figure II-9 Atmospheric Transmission Characteristics (Ref. 11)

D. REVIEW OF SOME RATIO TECHNIQUES

The use of a spectral ratio of 0.8 / 0.675 μm for determining the leaf area index for forest canopies was first reported in Reference 13. Thereafter, many different spectral ratios with various applications have appeared in the literature (Refs. 3, 4, and 14). In LANDSAT applications, the ratio of MSS 6 / MSS 5 (or 0.8 - 1.1 μm / 0.6 - 0.7 μm) was slightly more statistically significant than MSS 7 / MSS 5, but both ratios were useful in monitoring green biomass. The effectiveness of MSS 7 / MSS 5 or MSS 6 / MSS 5 ratio processing of agricultural data can be attributed in part to the strong spectral absorption of incident radiation by cholorophyll molecules over the range of 0.63 - 0.69 μm as shown in Figures II-1, II-2, and II-3. As to the spectral bandwidths used in the ratioing channels, limited studies showed that no substantial differences were found in regression significance among the infrared bandwidths of 0.75 - 0.8 μm, 0.80 - 0.90 μm, 0.80 - 1.00 μm, and 0.75 - 0.90 μm.

An oversimplified yet interesting illustration of how the LANDSAT MSS 7 - MSS 5 space can be divided into decision regions corresponding to various categories of interest is given by Reference 1 (see Fig. II-10). Notice that under certain conditions, the so-called soil line can be roughly established as shown in Figure II-10, with two extremes being flanked by clouds and cloud shadow. It is noted that the water is on the left side of the soil line while the vegetation is on its right side. The thresholded areas include all wild points, line dropping as well as snow and ice. A simple criterion, Perpendicular Vegetation Index (PVI), was devised to depict the soil line in the MSS 7 - MSS 5 space:

$$PVI = \frac{1}{2.6} (2.4\ MSS\ 7 - MSS\ 5)$$

The experimental results suggested that PVI = 0 indicates bare soil, a negative PVI indicates water, and a positive PVI indicates vegetation. Two different criteria, the Vegetation Index (VI) and the Transformed Vegetation Index (TVI), defined respectively as

$$VI = \frac{MSS\ 7 - MSS\ 5}{MSS\ 7 + MSS\ 5}$$

$$TVI = VI + 0.5$$

were reported to be able to compensate the signature variabilities due to the geographical locations and growth cycle deviations that would otherwise be introduced in the ratio of MSS 7 / MSS 5 or MSS 6 / MSS 5. A more sophisticated algorithm called SCREEN, capable of separating wild points, clouds, dense haze, water, and cloud shadow were recently reported in Reference 15, based on sun angle corrected and feature space rotated LANDSAT data.

As alluded to at the beginning of this report, the ratio techniques also have been employed in mineralogical mapping applications (Refs. 3 and 4). It was reported that the LANDSAT MSS band ratios of 4/5 (or 0.5 - 0.6 μm / 0.6 - 0.7 μm) and 6/7 were the least influenced by the vegetation cover on the rocks and thus would be more diagnostic of the spectral response of the ground. A strong absorption at 0.85 μm was found in the ferric iron. It was also suggested that the spectral region beyond 1.4 μm, especially between 2 and 2.5 μm, would contain more diagnostic spectral information on rock and soil types, primarily due to the low reflectance of green vegetation in this region.

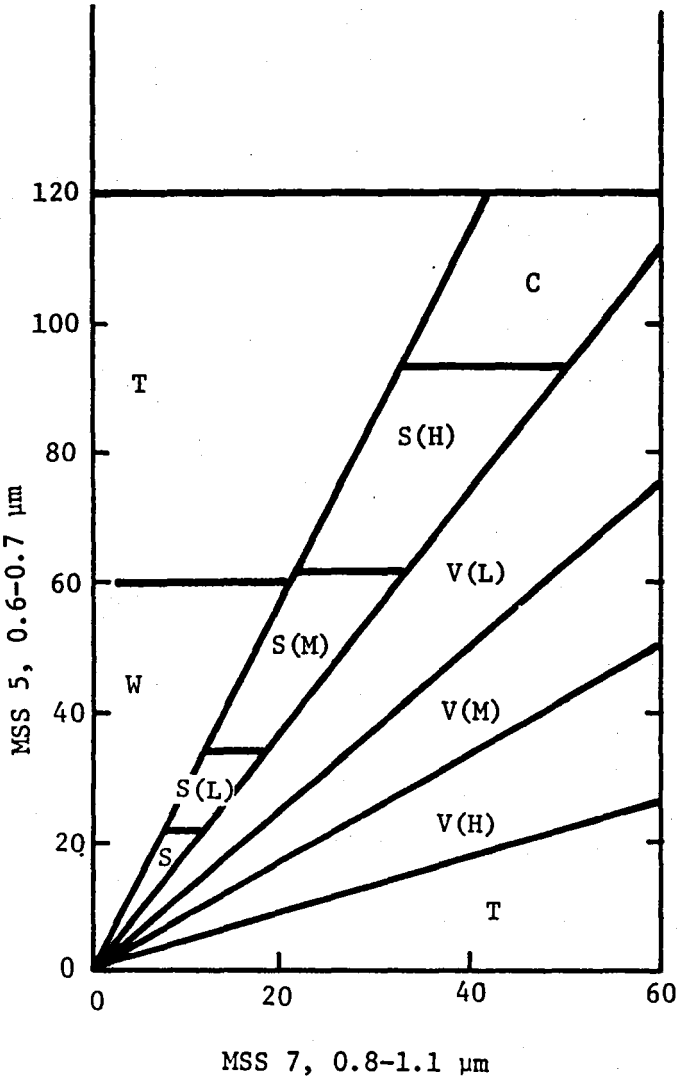

Legend:

C	Cloud
W	Water
S	Cloud Shadow
S(H)	High Reflecting Soil
S(M)	Medium Reflecting Soil
S(L)	Low Reflecting Soil
V(H)	High-Vigor Vegetation
V(M)	Medium-Vigor Vegetation
V(L)	Low-Vigor Vegetation
T	Threshold Categories Including Snow, Wild Points, etc.

Figure II-10 Scatter Diagram in LANDSAT MSS 7 - MSS 5 Space (Ref. 1)

E. CONCLUDING REMARKS AND RECOMMENDATIONS

The spectral reflectance characteristics of selected categories have been examined. Various ratio techniques in connection with green biomass monitoring, agricultural data processing, and mineralogical mapping have also been reviewed. The salient points in the preceding observations can be summarized as follows:

(1) There exist strong water absorption bands at 1.45 and 1.95 μm in the near IR region and one red chlorophyll absorption band at 0.65 μm in the visible spectrum that characterize the green vegetation reflectances.

(2) Lower moisture content in vegetation and soil equates to higher reflectances over the region of 0.5 - 2.6 μm.

(3) A strong 0.85 μm absorption band was found in the ferric iron.

(4) The spectral region beyond 1.4 μm, especially around 2 - 2.5 μm, was useful for detection of different rock types.

(5) The spectral bands of 1.55 - 1.75 μm and 2.10 - 2.35 μm were found to be very effective in differentiating between clouds and snow.

(6) LANDSAT MSS 5 (0.6 - 0.7 μm) was reported to be better than MSS 7 (0.8 - 1.1 μm) for snow and bare ground classification.

(7) The reflectance of clear water peaks at 0.42 μm, but sedimentation shifts this peak to the 0.52 - 0.58 μm region. This suggests that the latter spectrum region would be useful in monitoring water pollution problems.

(8) Because the water completely absorbs the near-IR wavelengths beyond 0.75 μm, it was reported that the 0.75 - 1.1 μm region could be very effective in delineation of the land-water boundaries.

(9) The only thermal IR band used in the Skylab EREP, 10.2 - 12.5 μm, was reported to be relatively effective in agricultural data processing.

(10) The LANDSAT MSS ratios of 6/5 or 7/5 were found to be very sensitive to green biomass.

(11) More sophisticated criteria like the vegetation index (VI) or Bayesian classification may be needed to account for crop signature variabilities due to the different geographical locations, growth cycle deviations, and physical phenomena that could not be discerned by simple ratio processing.

It should be clear from the discussions thus far that there is no single spectral ratio capable of discriminating between all categories of interest.

Furthermore, due to the many variables associated with each category such as varying sediment loads in water, snow of various natural aging, soils of different moisture levels, and vegetation of everchanging growth stages, even the best spectral ratio has its limitation of discriminatory power. Nevertheless, the ratio techniques seem to be able to alleviate some undesirable atmospheric effects, rendering the spectral ratios preferable to single spectral bands used separately.

In view of the preceding arguments, the following spectral regions are recommended for use in the spectral ratio processing of satellite image data for the categories of vegetation, soil, water, clouds, snow, ice, and some minerals:

1) Spectral regions centered at .65 μm and .85 μm for separation of water, bare earth, and vegetation from clouds, snow, and ice.

2) A spectral region centered at 1.55 μm for separation of clouds from snow and ice.

3) A spectral region centered at 1.2 μm for a possible separation of snow from ice.

The appropriate decision thresholds required to classify vegetation, bare earth, water, and clouds/snow/and ice were determined for FILE-I through computer simulation and published in Reference 17.

For the definition of FILE-II, the spectral signature analysis computer programs were used to determine how the signatures of typical targets vary in the absence of contaminating factors. This was done to determine whether the algorithm for classifying features should involve simple ratio tests of the form:

$$V_{ir} > a \cdot V_{vr}$$

or the more general test:

$$V_{ir} > a \cdot V_{vr} + b$$

where b is an offset voltage, a is a constant, and V_{ir} and V_{vr} are the infrared and visual red camera output voltages, respectively. The analysis was motivated by the fact that the more general test appears to work better with real flight data obtained from the FILE-I aircraft flight test.

The analysis shows that there is, indeed, a theoretical basis for using the latter test. It was established that, in the absence of contaminating factors such as pixel response nonuniformity, noise, dark signal, and the like, the camera output variation with changes in sun angle is different in the two spectral bands. This implies that the ratio that best separates features is a function of sun elevation, and the more general form above provides the best linear approximation to the optimum decision function.

This fact is illustrated by Table II-1, which tabulates the variation in red/infrared ratio with solar zenith angle (the angle between the sun's rays and local vertical).

The analysis was done for 18 feature types and visibilities of 5 and 23 km. In all cases variation of ratio with sun angle was observed, though it is generally small (10-15%). In the original analysis, where contaminating factors were considered, this small variation was not readily perceived.

The conclusion drawn is that somewhat better performance can be expected with the more general algorithm. Still better performance should be possible if the decision parameters are made to be functions of sun angle. The achievable improvement depends on how large the contaminating factors are compared to the variation in red/infrared ratio.

The optimum value of "b" for each decision threshold is not readily determined analytically. This is so because it accounts for a second-order effect that is easily masked by such factors as camera pixel-response non-uniformity, the nature of the terrain (hilly versus flat), the range of sun angles expected for the portion of mission using a particular threshold parameter set, season of the year, camera dark signal, camera optical system effects (such as reduced image brightness at the edge of the image), and the like. The value that minimizes errors will depend on all these factors to some extent. In principle, optimum parameter values can be derived for a given mission or set of missions by analysis of these factors. In practice, however, the data base for such an analysis does not exist. Further, the analysis would be complicated--it cannot be expressed as a simple formula. The recommended approach, therefore, is to establish the parameters empirically through analysis of the data from the FILE IB aircraft flight test. This analysis will also provide a portion of the needed data base for analytical optimization for future missions.

Table II-1. Signature Variation with Sun Angle

Feature, Visibility	Sun Angle	V_{vr}	V_{ir}	Ratio V_{vr}/V_{ir}
Cloud, 5 km visibility	0	4.20	4.12	1.02
	10	3.83	3.95	.97
	20	3.48	3.69	.94
	30	3.12	3.36	.93
	40	2.72	2.95	.92
	50	2.27	2.47	.92
	60	1.78	1.93	.92
	70	1.24	1.34	.93
Black earth, 5 km visibility	0	1.01	.74	1.36
	10	.69	.62	1.11
	20	.48	.51	.94
	30	.36	.43	.84
	40	.28	.36	.78
	50	.23	.30	.77
	60	.19	.24	.79
	70	.15	.18	.83

Figure II-11a illustrates the decision boundaries in terms of the .65 μm and .85 μm camera outputs.

The decision thresholds used for separation of clouds, snow, and ice were determined empirically through analysis of data contained in various literature sources previously described. Figures II-11b and II-11c illustrate the classification boundaries used for these features.

(a) INITIAL CLASSIFICATION FOR ALL PIXELS

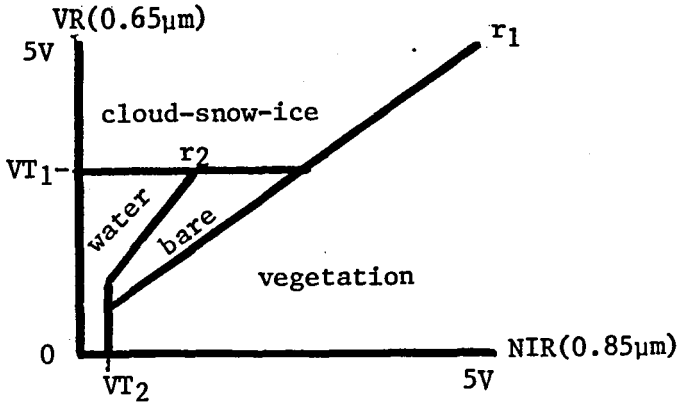

VT_1 = 1.15V for low sun angle
= 1.90V for high sun angle

VT_2 = 0.45V for low sun angle
= 0.73V for high sun angle

r_1 - VR = 0.694 NIR + b_1 b_1 = 0.2 Volts

r_2 - VR = 1.18 NIR + b_2 b_2 = 0.1 Volts

(b) CLASSIFICATION BETWEEN CLOUD AND SNOW/ICE PIXELS

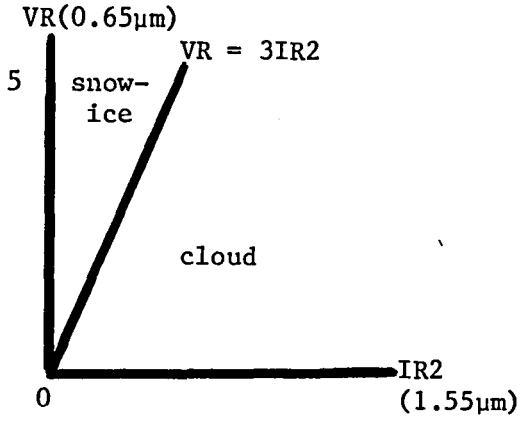

(c) CLASSIFICATION BETWEEN SNOW AND ICE PIXELS

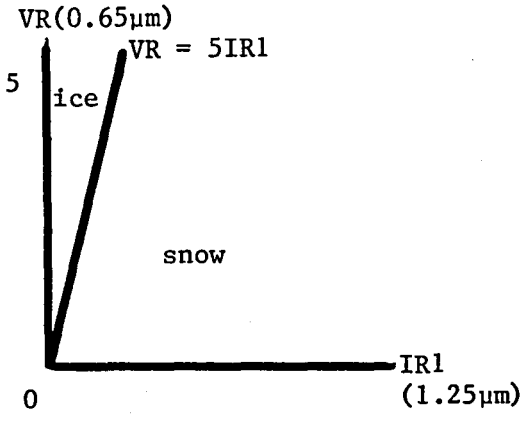

All slopes, thresholds, and biases will be made adjustable in the hardware to accommodate algorithm changes due to FILE-IB data analysis results, VILAT-III studies, and IR radiometer field test data.

Figure II-11 Recommended FILE-II Classification Algorithm

REFERENCES

1. A. J. Richardson and C. L. Wiegand, "Criteria for Distinguishing Vegetation from Soil Background Information and Their Use in Processing LANDSAT MSS Data," Agricultural Research Service, USDA, Weslaco, Texas 1976.

2. C. J. Tucker, "Use of Near Infrared/Red Radiance Ratios for Estimating Vegetation Biomass and Physiological Status", NASA TMX-71388, July 1977.

3. L. C. Rowan, A. F. H. Goetz, and R. P. Ashley, "Discrimination of Hydrothermally Altered and Unaltered Rocks in Visible and Near Infrared Multispectral Images," Geophysics, Vol. 42, No. 3, April 1977.

4. B. S. Siegall and A. F. H. Goetz, "Effect of Vegetation on Rock and Soil Type Discrimination," Photogrammetric Engineering and Remote and and Sensing, Vol. 43, No. 2, February 1977.

5. P. L. Johnson, Ed., "Remote Sensing in Ecology," University of Georgia Press, Athens, Georgia 1969.

6. J. M. Johnson, et al., "Utilization of LANDSAT Data for Water Quality Surveys in the Choptank River," NAS Earth Resources Survey Symposium, Vol. I-D, Houston, Texas, June 1975.

7. W. G. Driscoll, Ed., "Handbook of Optics," McGraw-Hill, New York, New York 1978.

8. D. F. McGinnis et al., "Factors Affecting Snow Assessment from LANDSAT Data," Proc. NASA Earth Resources Survey Symposium, Houston, Texas, June 1975.

9. J. C. Barnes and M. D. Smallwood, "Snow Survey from Space, with Emphasis on the Results of the Analysis of Skylab EREP S192 Multispectral Scanner Data," Proc. NASA Earth Resources Survey Symposium, Houston, Texas, June 1975.

10. J. A. VanAllen, Ed., "Scientific Uses of Earth Satellites," The University of Michigan Press, Ann Arbor, Michigan 1956.

11. "Skylab Earth Resources Data Catalog," NASA/JSC, Houston, Texas 1974.

12. C. H. Chang, "Skylab S192 Data Evaluation: Comparisons with ERTS-1 Results," Lockheed Electronics Co., LEC-1711, Houston, Texas 1974.

13. C. F. Jordan, "Derivation of Leaf Area Index from Quality of Light on the Forest Floor," Ecology, Vol. 50, No. 4, April 1969.

14. R. M. Killen, "Channel Ratio Processing," LEC-7780, Lockheed Electronics Co., Houston, Texas, March 1976.

15. P. F. Lambeck, "Signature Extension Preprocessing for LANDSAT MSS Data," ERIM 122700-32-F, ERIM, Ann Arbor, Michigan, November 1977.

16. R. T. Schappell, et al., "Experimental and Simulation Study Results for Video Landmark Acquisition and Tracking Technology," Final Report of NASA Contract NAS1-14489, NASA Contractor Report 158997, February 1979.

CHAPTER III IR CAMERA DEFINITION

A. OVERVIEW

In order to implement the cloud detector described in Chapter II it is necessary to obtain a sensor which operates in the bands centered at wavelengths greater than 1.1 μm. The cameras developed for FILE-I are not useful for this. This chapter describes the preliminary development effort including the results of a survey of IR detectors, construction of an IR radiometer with the selected detector, field tests to verify the simulated spectral characteristics, and finally a top-level definition of the camera to be flown on FILE-II

B. IR DETECTOR SURVEY

Selection of an appropriate IR detector for the specific FILE-II experiment requirements and cost constraints required a considerable tradeoff, because even with the large number of available IR detectors, none was usable as an off-the-shelf component. The following constraints were considered in order of importance in the selection of a detector:

1) Since implementation of the cloud/snow discrimination algorithm discussed in Chapter II required imagery in the spectral region around 1.55 μm, this was the primary constraint for selecting a specific detector.

2) Operating at room temperature greatly simplifies the infrared system since it would not be necessary to implement a cooling system. This also will keep the system costs to a minimum.

3) One of the initial objectives of this task was to find a method of reusing the breadboard cameras from the FILE-I experiment in order to minimize development costs. To achieve this goal it would be necessary to develop a detector array, with operating capabilities in the IR regions of interest, that was compatible with the FILE-I arrays. In order to be compatible it is necessary that the array consist of at least 100 linear elements with similar response characteristics. A 100 x 100 element area array would be the ideal detector size to use.

4) Projected development costs were another major factor.

Table III-1 summarizes the characteristics of potential detector materials considered. This information was extracted from References 1 through 20.

Review of Table III-1 shows that both a germanium detector array and a lead sulphide detector array would satisfy the system requirements. Of these two detector choices, the germanium detector offers both a faster response time and a higher detectivity value. Discussions with Judson Infrared Inc. indicated that they could supply a germanium detector

Table III-1 Infrared Detector Survey

Detector	Operating Temp, K	Wavelength Range, μm	Peak Wavelength, μm	Detectivity (D*) @ Peak	Detectivity (D*) @ 1.55 μm	Response Time, s
Germanium Photodiode	300	1.0 - 1.8	1.5	1×10^{11}	1×10^{11}	0.1
Germanium Photodiode	77	0.9 - 1.8	1.6	2×10^{14}	2×10^{14}	-
Lead Sulphide	300	0.5 - 3.5	2.5	1×10^{11}	8×10^{10}	300
Lead Sulphide	193	0.7 - 4.0	2.8	7×10^{11}	4×10^{11}	200
Lead Sulphide	77	0.7 - 4.8	3.1	2×10^{11}	8×10^{10}	-
Lead Selenium	298	1.0 - 4.6	3.3	4×10^{9}	2×10^{9}	-
Lead Selenium	77	1.0 - 7.0	5.0	2.5×10^{10}	7×10^{9}	20
Indium Arsenic	298	1.4 - 3.3	3.0	5×10^{9}	4×10^{8}	-
Indium Arsenic	77	1.2 - 2.8	2.7	7×10^{11}	2×10^{11}	5
Indium Antimonide	80	1.5 - 5.2	5.0	1×10^{11}	2×10^{10}	.2
Indium Antimonide	78	1.0 - 5.5	-	3×10^{11}	-	.5
Mercury Cadium Telluride	298	1.0 - 3.1	2.9	1×10^{10}	6×10^{9}	-
Mercury Cadium Telluride	77	8.0 - 15	-	-	-	-
Lead Tin Telluride	77	1.0 - 11.0	10.0	1×10^{11}	-	-
Pyroelectric	300	-	-	1×10^{9}	1×10^{9}	100
Triglycine Sulfate	300	-	-	1×10^{9}	1×10^{9}	-
Thermopile	300	-	-	2×10^{8}	2×10^{8}	-
Thermister Bolometer	300	-	-	3×10^{8}	3×10^{8}	-

(photovoltaic), operating at 300°K, with a peak response occurring at 1.55 μm, and a response time of .1 microseconds.

Although focal plane array technology has progressed rapidly in recent years, even the most advanced array approach, the monolithic extrinsic array, has not been developed sufficiently to allow fabrication of IR area arrays compatible with the FILE-I 100 x 100 arrays.

The monolithic intrinsic approach is a technology with long-term potential, but is presently limited by the lack of a mature infrared materials technology and thus remains the least developed of the approaches. The current NASA sponsored development effort to fabricate and develop indium antimonide CCD technology is addressing a number of critical infrared materials problems. Progress, however, is expected to be slow, reflecting the formidable infrared materials and processing issues. Small indium antimonide TDI area arrays with a few hundred elements may become available in a few years.

The CID approach provides only a limited potential for area arrays larger than 32 x 32 because of the output capacitance limitations.

The hybrid CCD arrays represent an attractive approach, especially for the FILE applications. Significant advances have been made both in the development of intrinsic photovoltaic detector arrays and the required interconnect technology. A new generation of high density CCD multiplexers, to which these arrays will be coupled, will be available in a few years. This hybrid approach may be optimum for FILE-II in that it provides the best of a mature infrared detector technology and the well developed silicon CCD technology.

The germanium detector was selected for the acquisition of field data to demonstrate the feasibility of cloud/snow discrimination. This decision was based on the higher detectivity of germanium in the region of interest, faster response time, and an available vendor.

C. VILAT IR RADIOMETER

The results of Chapter II demonstrate that there is evidence to believe that spectral measurements taken at 1.55 μm would provide the necessary information to distinguish clouds from snow and ice. Furthermore, the earlier portion of this chapter concluded that germanium could be used as a detector in this region. Under this task an IR radiometer (Figure III-1) was designed and manufactured to study classification of clouds, snow, and ice.

The radiometer detector consists of a $1mm^2$ germanium photo-diode obtained from Judson Infrared. The optics consist of a 60 mm focal length achromat with a F Stop of 3.75. In this arrangement, the total field of view is approximately 1°. Provisions were made so that filters could be easily interchanged. The seven interference type filters that are currently available with the instrument are listed in Table III-2.

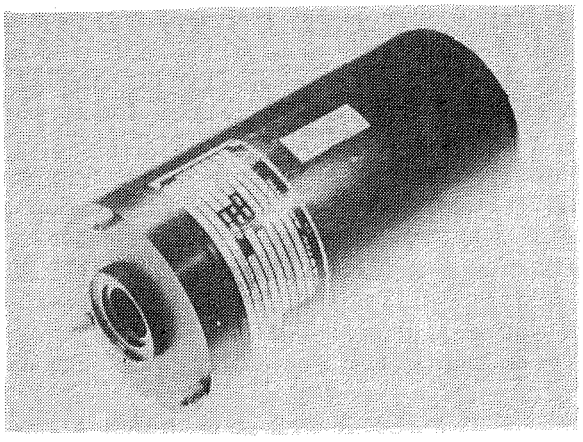

Figure III-1 VILAT Breadboard IR Radiometer

Table III-2 IR Radiometer Filter Characteristics

Filter (Nominal Wavelength)	Peak Transmission (Percent)	Peak Wavelength (micrometers)	Half-power Bandwidth (micrometers)
1.1	21.0	1.127	0.058
1.2	31.3	1.214	0.036
1.3	31.7	1.314	0.042
1.4	22.5	1.418	0.046
1.5	21.7	1.518	0.115
1.6	22.7	1.618	0.090
1.7	29.0	1.703	0.070

The radiometer was designed to produce a maximum output of approximately 8 volts when viewing bright clouds. The instrument has a peak-to-peak error of ±2% of full scale with direct readings and less than ±1% with dark voltage compensation.

D. VILAT IR RADIOMETER FIELD TEST RESULTS

Field tests have been conducted with germanium IR radiometer described in the previous section. Spectral signatures of clouds, granular, snow, vegetation, water, and rocks have been acquired in the Colorado mountains around Loveland Pass and Dillon Reservoir and in the vicinity of the Martin Marietta Waterton facility. The data are summarized in Tables III-3 and III-4.

Quantitatively, the signatures agree with those expected. Specifically, the measurements confirm the fact that a ratio of radiance at 1.55 μm to radiance at a shorter wavelength can distinguish clouds from snow. The radiance dip at 1.4 μm due to atmospheric water vapor absorption is quite pronounced. Results of the field tests have been compared with published reflectance data and calibration target reflectance curves in order to confirm the cloud detector concept. The spectral signature of snow obtained with the radiometer is graphically illustrated in Figure III-2. Comparison of this data provides strong evidence that cloud/snow discrimination can be performed in a band centered at 1.55 μm.

E. IR CAMERA DEFINITION

Based on the discussion in Chapter II and in Sections B, C, and D of this chapter, a spectral band of 1.55 - 1.75 μm was found to be very effective for differentiating between clouds and snow or ice. Furthermore, germanium and lead sulphide detectors appear to be the best suited for FILE-II application due to greater detectivity and faster response time. However, neither of the detectors discussed in Section B is available in 100 x 100 element arrays or any linear array that is compatible with the 100 x 100 FILE-I cameras. Therefore, a design of the IR camera was deemed necessary.

Table III-3 Spectral Signatures from Field Tests

CLEAR DAY SPECTRAL RADIANCE $mw \cdot sr^{-1} \cdot cm^{-2} \cdot \mu m^{-1}$ - with Sun Near Zenith							
FEATURE	1.1μm	1.2μm	1.3μm	1.4μm	1.5μm	1.6μm	1.7μm
Granular snow at 4°C near Loveland Pass, Colorado Elevation: 3655 m.	2.31	1.21	0.842	0.386	0.253	0.310	0.242
Same as above, different sample	2.89	1.76	1.24	0.452	0.357	0.430	0.366
Water, viewed approx. 75° from normal to surface	0.742	0.807	0.630	0.392	0.450	0.570	0.468
Cloud (Average of multiple readings)	5.81	7.73	4.72	1.17	1.93	3.96	3.21
Healthy green bushes	6.27	5.87	4.14	1.12	1.52	2.19	1.89
Red rock (sandstone)	3.95	3.85	2.76	1.23	1.94	2.53	2.17
Dry green grass (distressed)	6.66	5.96	4.20	1.33	1.69	2.72	2.34

NOTE: Rapid variations of radiance with wavelength are smoothed to some extent by filter bandwidth. Half-power bandwidths were 36 to 115 nm, depending on band.

Table III-4 Data of Table XIV Normalized with Respect to 1.55 um Radiance

FEATURE (See Table III-3)	NORMALIZED SPECTRAL RADIANCE						
	1.1	1.2	1.3	1.4	1.5	1.6	1.7
Snow #1	8.21	4.30	2.99	1.37	0.899	1.10	0.860
Snow #2	7.34	4.47	3.15	1.15	0.907	1.09	0.930
Water	1.45	1.58	1.24	0.769	0.882	1.12	0.918
Cloud	1.76	2.62	1.60	0.397	0.655	1.345	1.090
Bushes	3.38	3.16	2.23	0.604	0.819	1.18	1.02
Red rock	1.77	1.72	1.23	0.550	0.868	1.13	0.971
Dry grass	3.02	2.70	1.90	0.603	0.766	1.23	1.06

(Note: 1.55μm radiance is taken to be the average of 1.5μm and 1.6μm radiances)

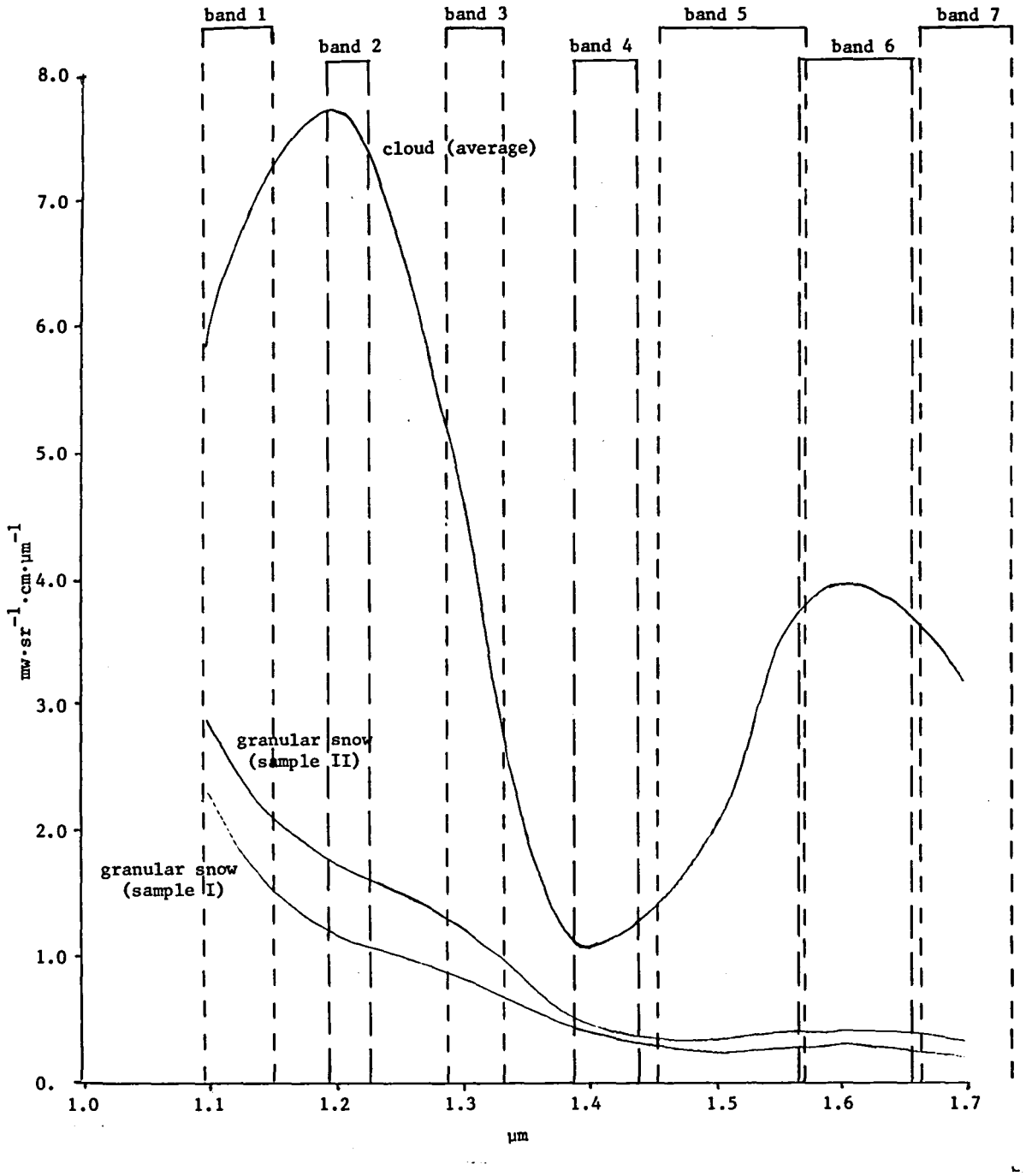

Figure III-2 Spectral Signatures of Clouds and Snow Based on Field Measurements

Presently available detectors consist of non-integrated detectors. That is, each detector element in an array is totally independent of the surrounding elements and no provision is made for extracting the detector element data. When the number of elements in the array is large, this creates a serious interface problem. Work is being done to solve this problem by manufacturing charge coupled device (CCD) detector arrays of materials that are infrared sensitive. However, these devices are several years away due to the lack of experience in semi-conductor manufacturing with materials other than silicon. One interim solution would be to utilize existing silicon circuits combined with a detector deposition process to consolidate present integrated circuit and infrared detector technologies.

The integrated circuit that could be most readily adapted to this concept is manufactured by Reticon of Sunnyvale, California. The circuit is a solid-state scanner which is available in linear arrays of 64, 128, 256, 384, or 512 elements and a 100 element by 100 element square array. The circuits are basically identical with the exception of the number of elements. Figure III-3 is an equivalent circuit of the solid-state scanner. Each cell consists of a photodiode detector and a parallel storage capacitor and is connected through an MOS transistor switch to a common video output line. The switches are turned on and off in sequence by the shift register scanning circuit.

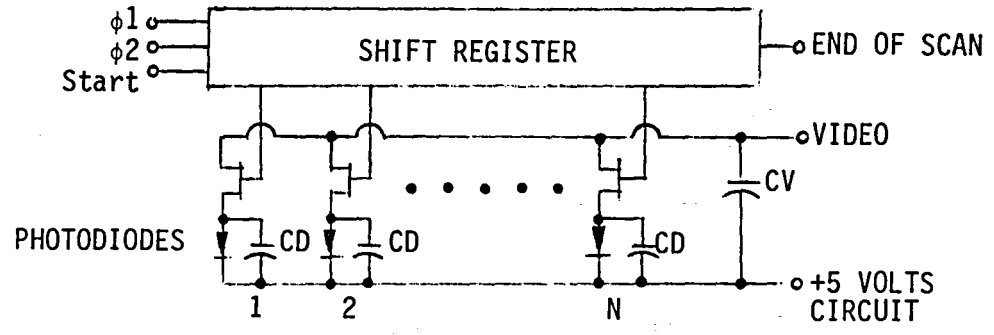

Figure III-3 Scanner Equivalent Circuit

The required circuit modification would consist of eliminating the photodiodes and capacitors and providing a pad for connection to a lead sulphide array. Figure III-4 shows the modified equivalent circuit.

The deposition of the lead sulphide detectors can be done by Optoelectronics of Petaluma, California. The lead sulphide detectors are photoconductive so detector impedance is a function of the light intensity.

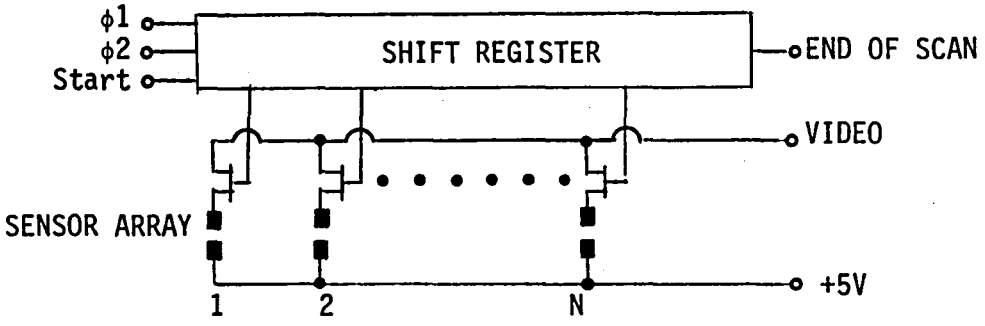

Figure III-4 Modified Equivalent Circuit

The multiplexed detector array can be converted to a video signal with a transimpedance amplifier. Figure III-5 shows a typical circuit. The clock generator provides the clocking necessary to scan the sensor array, and the amplifier conditions the output. Register R1 sets the gain while Register R2 biases out the dark signal.

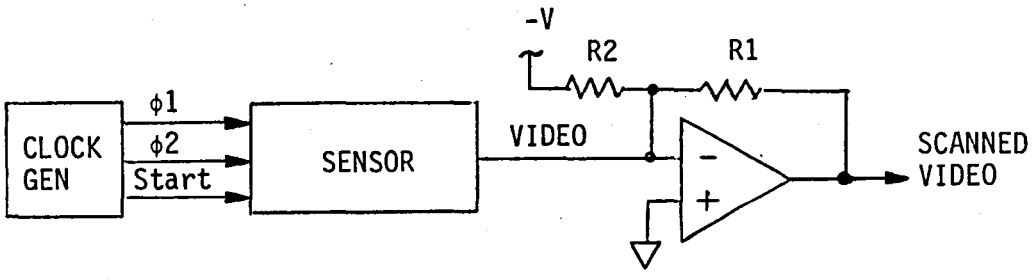

Figure III-5 Typical Transimpedance Amplifier

The uniformity of deposited lead sulphide is not very good, which would make a 100 x 100 array prohibitive. A 100-element linear array with mechanical scan could be utilized to minimize the number of elements.

A second approach, which appears to be significantly better, is a germanium array with the multiplexer described above or a hybrid scanner. A 10,000 (100 x 100 detectors) input scanning device would not be realistic for hybrid construction. Therefore, a 100-element linear array with mechanical scan was considered. A 100-element linear germanium array can be provided by Judson Infrared, Inc. The array will be mounted on a hybrid substrate and interconnected to a scanning circuit. Figure III-6 shows a

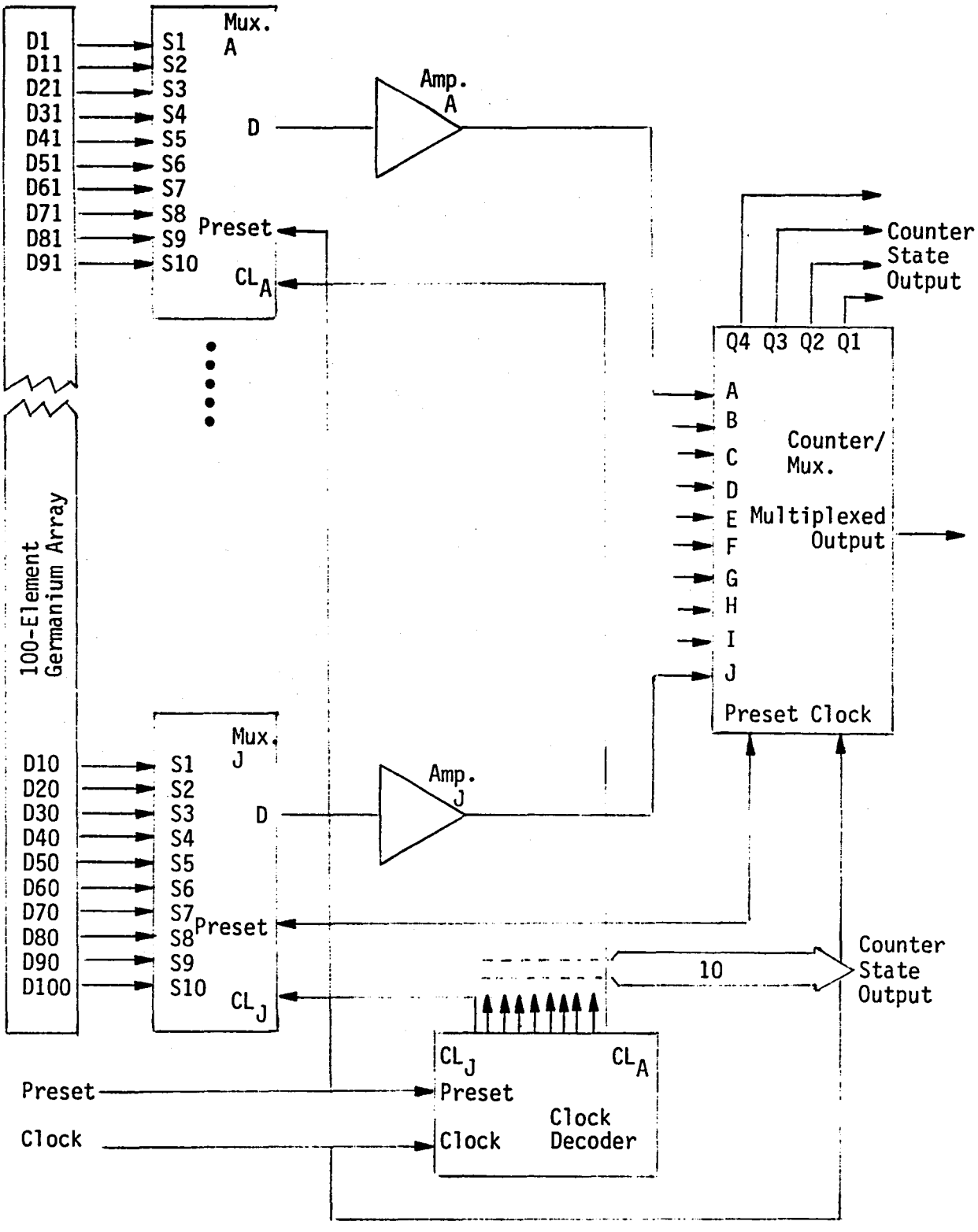

Figure III-6 100-Element Linear Array Germanium Detector

preliminary design for the germanium hybrid detector. The scanning circuit consists of 51 off-the-shelf IC chips plus amplifier passive components. The entire detector array can be fabricated in a 2-inch square hybrid package with an optical window. The alternate approach using the Reticon multiplexer would result in a smaller package.

Of the two candidate concepts, the germanium detector was selected because of faster response time, higher detectivity value, and less risk due to dependance on outside vendors. It is interesting to note that the Westinghouse Defense and Space Center, while under contract to SAMSO to investigate cloud/snow discrimination, also chose the Judson germanium detector.

One of the advantages of a mechanically scanned linear array is closed-loop dark level compensation. The linear array output, when exposed to a "black line," can be digitized and stored. The dark levels can then be subtracted from the live scene during data acquisition. This would be done on every image and would accurately cancel out the dark level for each pixel element.

The definition of the integrated camera system is discussed in more detail in Chapter V entitled, "FILE-II Preliminary Definition."

REFERENCES

1. Chang, Dr. C. Y., "Multispectral Ratioing for Remote Sensing," MCR-79-531, Martin Marietta Corporation, February 1979.

2. Levinstein, Henry and Mudar, J., "Infrared Detectors in Remote Sensing," Proceedings of the IEEE, Volume 63, No. 1, January 1975.

3. Levinstein, Henry, "Infrared Detectors," Physics Today, Volume 30, November 1977.

4. Jacobs, Stephen F., "Handbook of Optics," Optical Society of America, Section 4, McGraw Hill, 1978.

5. Putley, E. H., "Modern Infrared Detectors," Physics in Technology Section 4, pages 202-222, December 1973.

6. Hudson, Richard J., "Infrared System Engineering," John Wiley and Sons, New York, 1969.

7. Zwerdling, S.; Smith, R. A.; and Theriault, J.P., Infrared Physics, Section 8, pages 271-336, 1968.

8. Chen, Jar-Mo, "Infrared Detector Survey," Electro-Optical Systems Design, August 1975.

9. Zwicker, H. R., "Photoemissive Detectors, Topics in Applied Physics," Volume 19, Optical and Infrared Detectors, Springer-Verlag, 1977.

10. Putley, E. H., "Solid State Devices for Infrared Detection," Journal of Scientific Instrumentation, 43, pages 857-868, December 1966.

11. Santa Barbara Research Center Brochure, Santa Barbara Research Center, Goleta, California, 1975.

12. Judson Infrared Inc., Brochure, Series J-16, Judson Infrared Inc., Ft. Washington, Pennsylvania.

13. Ando, K. J., "Assessment Study of Infrared Detector Arrays for Low Background Astronomical Research", NASA-CR-152169, August 1978.

14. Thom, R. D.; Eck, R. E.; Phillips, J. D.; and Scorson, J. B., InSb CCDs and Other MOS Devices for Infrared Applications," Proceedings of International Conference on the Application of Charge Coupled Devices," October 1975.

15. Kim, J. C., "InSb MOS Detector", GE Army Night Vision Laboratory, Report Number AD-B004428L, February 1975.

16. Ceeung, D. T.; Tennant, W. E.; Barrowcliff, E. E.; Rode, J. P.; Gertner, E. R.; and Andrews, A. M., "MIS Studies on Narrow Bandgap III-V Compounds," Proceedings IRIS, July 1976.

17. Thom, R. D.; Koch, T. L.; and Parrisn, W. J., "Indium Antimonide Infrared CCD Linear Imaging Arrays with On-Chip Preprocessing," Paper No. 78-1728, presented at AIAA/NASA.

18. Kim, J. C., "InSb Charge-Injection Device Imaging Array, "IEEE Transactions on Electron Devices," ED-25, page 232, 1978.

19. Milton, A. F., "Charge Transfer Devices for Infrared Imaging," "Topics in Applied Physics," Volume 19, Optical and Infrared Detectors, Springer-Verlag, 1977.

20. Stebbins, William J., "Snow/Cloud Discrimination Staring Mode Radiometer," presented at Electro-Optics Lanser Conference, September 1978.

CHAPTER IV VILAT PROCESSOR AND GROUND SUPPORT EQUIPMENT

In the implementation of the FILE-I algorithm, the control and classification logic was not complex enough to warrant a general purpose processor. However, as the scope of FILE experiments increases to include additional classification, correlation, pointing and tracking, and navigation capabilities, the need for such a processor is unquestionable. Therefore, a digital signal processor was designed, built, and tested to provide the basis for future FILE systems. The actual design of the VILAT processor has been previously documented in the VILAT-I final report (Ref. 1).

In addition to the VILAT processor, it was established that an additional FILE Ground Support Equipment (GSE) test set was required for FILE-II because the original set is dedicated to the Shuttle flight test of FILE-I. This chapter describes the development of the processor and the second GSE.

A. VILAT PROCESSOR

The goal of this task was to design a processor with an expandable instruction set to allow hardware or microcoded implementation of correlation, image classification, tracking, navigation, and related functions that may be required for future FILE concepts. To achieve the desired flexibility, the processor was designed around an Advanced Micro Devices 2900 chip set. The microprogrammability provided by this design approach allows a virtually unlimited instruction set for rapid control of special hardware functions and replacement of random-logic in portions of the system where speed is less critical.

The processor has become the heart of the FILE-II system, and in this capacity has greatly reduced the amount of circuit design, building and testing required and has provided the additional advantage of flexibility compared with a random logic design. Figure IV-1 is a block diagram of the processor. The processor, shown in Figure IV-2, has eight general-purpose registers and eight addressing modes, a 16-bit word for both instructions and data, memory-mapped I/O and in the initial version 16k words of read-write memory. In addition, a "virtual control panel" program in read-only memory provides the functions of memory examination and alteration, loading and saving programs and data, initiation of program execution, and debugging utilities. The read-write memory is being expanded for FILE-II to 56k words. Although the initial instruction set is tailored to basic arithmetic and logic operations, text can be handled with the instructions provided. A summary of these instructions is provided in Table IV-1.

A cross-assembler was written to facilitate programming of the processor. The assembler was written in FORTRAN, and is modular in design and table-based to maximize flexibility for adding new instructions and/or running on other computers. Features of the assembler include:

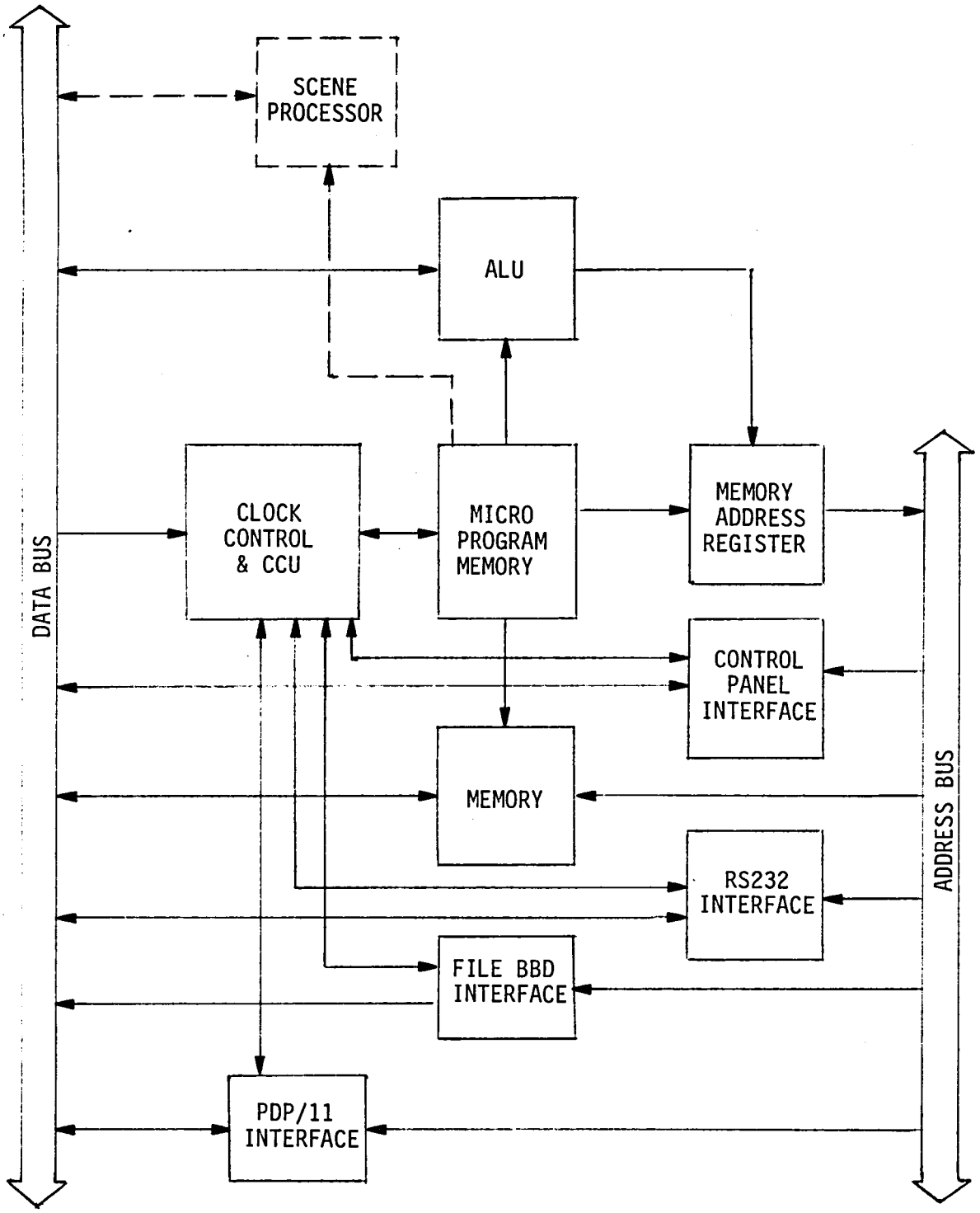

Figure IV-1 Processor Block Diagram

Table IV-1 VILAT Processor Instruction Set

Mnemonic	Description
CLR	Clear register or memory location
COM	Complement (1s) register or memory location
INC	Increment register or memory location
DEC	Decrement register or memory location
NEG	Complement (2s) register or memory location
TST	Test register or memory location
ROR	Rotate right register or memory location
ROL	Rotate left register or memory location
ASR	Arithmetic shift right register or memory location
ASL	Arithmetic shift left register or memory location
ADC	Add carry to register or memory location
SBC	Subtract carry from register or memory location
SXT	Sign extend register or memory location
NOV	Move register to register, register to memory location, or memory location to register
CMP	Compare register to register or register to memory location
ADD	Add register, register and memory location, or memory locations
SUB	Subtract registers, register and memory location, or memory locations
BIT	Bit test (AND) registers, register and memory location, or memory locations
BIC	Bit Clear (A · B) registers, register and memory location or memory locations
BIS	Bit set (OR) registers, register and memory location, or memory locations
XOR	Exclusive OR registers, register and memory location, or memory locations
BR	Unconditional branch
BNE	Branch if not equal zero
BEQ	Branch if equal to zero
BPL	Branch if plus (or zero)
BMI	Branch if minus
BVC	Branch if overflow clear
BVS	Branch if overflow set
BCC	Branch if carry clear
BCS	Branch if carry set
JMP	Unconditional jump
JSR	Jump to subroutine
RTS	Return from subroutine
MARK	Mark (aid in subroutine return)
HALT	Halt
NOP	No operation
CLC	Clear carry status bit
CLV	Clear over-range status bit
CLZ	Clear zero status bit
CLN	Clear negative status bit
CCC	Clear all status bits
SEC	Set carry status bit
SEV	Set over-range status bit
SEZ	Set zero status bit
SEN	Set negative status bit
SCC	Set all status bits

(1) symbols may be of arbitrary length;

(2) arithmetic, logical operations and shifts may be used in any expression;

(3) pseudo-operations are provided to format listings and facilitate programming;

(4) constants may be expressed in any number base from 2 to 16; and

(5) alphabetized symbol tables and meaningful error messages are provided to facilitate error correction.

Input/output operations are performed either by polling or by quasi-DMA (direct-memory access). Initially the I/O capabilities consist of two serial interface ports for RS-232-Compatible communications, a general-purpose parallel port, a FILE-I breadboard system interface to receive classified imagery from FILE-I television cameras, and control panel interfacing for manual halting, single-stepping, displaying or altering memory contents, invoking user programs and loading and saving programs and data. For the FILE-II system quasi-DMA ports are being added for video input and camera control and interfacing to a 9-track tape unit. In addition, interfaces for a television image display and special control panel are being provided. One of these utilizes the parallel port of the original design.

The basic processor cycle time is 200 ns. Register-to register addition and data movement are performed in 600 ns; and memory-to-memory addition data movement requires 1.2 and 1.0 μs, respectively. Multiplication and division are currently done in software, although the flexibility to implement these operations in microcode or hardware has been provided. Multiplication, division, character I/O, task scheduling and similar generally useful routines are being placed in the read-only memory for ease of use in future applications.

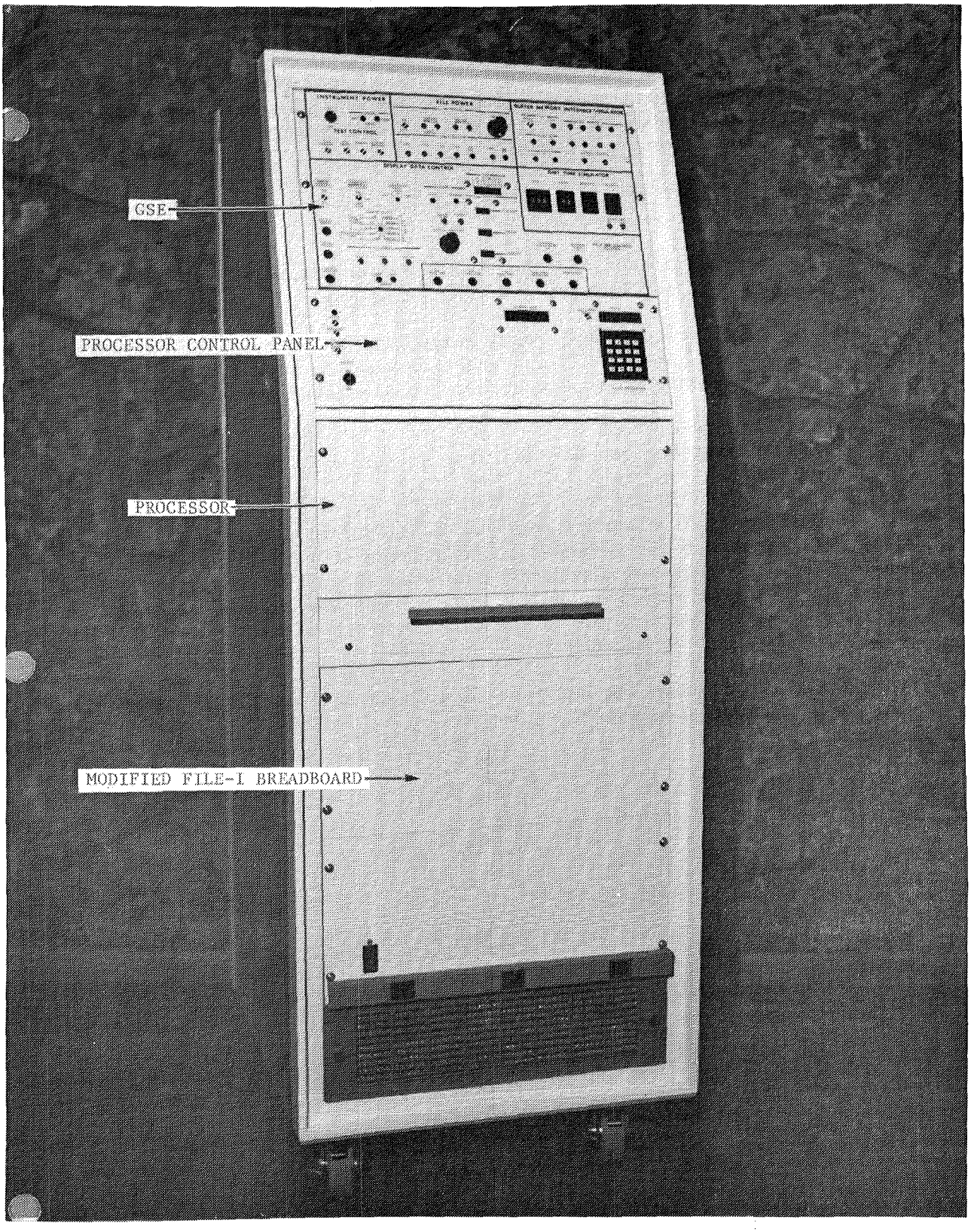

Figure IV-2 VILAT (Video Landmark Acquisition and Tracking) Processor and Test Equipment

B. SECOND FILE-I GROUND SUPPORT EQUIPMENT SET

A second GSE test set was built to allow operation of the FILE-I breadboard system. This was necessary because of the fact that the original set was required at Kennedy Space Center for FILE-I integration into the OSTA-1 pallet in preparation for flight.

The second test set is electrically identical to the original except that:

(1) Image simulator and sun simlator controls were deleted because they are not required for the breadboard.

(2) Additional display capabilities were added to allow operation with a third camera. This change was made to permit cloud detection experiments to be conducted with simulated imagery.

These changes did not affect compatibility with the FILE-I flight hardware. Either test set can be used with either the breadboard system or the flight hardware.

Mechanically, the second test set is different due to a different intended use. The first set was intended to be a piece of portable test equipment, while the second set was expected to be used as part of a system. The latter was therefore made rack-mountable, panel layout was altered slightly, and the larger connectors were moved to the back of the equipment to simplify interconnections in a rack-mounted configuration.

Figure IV-2 shows the set installed in an equipment rack along with the digital processor and support equipment.

C. REFERENCES

1. R. T. Schappell, et al., "Experimental and Simulation Study Results for Video Landmark Acquisition and Tracking Technology," NASA CR 158997, February 1979.

CHAPTER V FILE-II PRELIMINARY DEFINITION

One of the primary functions of this contract was to define, on a preliminary basis, the FILE-II system. Chapters II through IV have already summarized the studies and development effort leading up to the experiment definition. This chapter describes the definition of the FILE-II experiment resulting from these studies.

It is appropriate at this time to review the goals of the experiment and to summarize the results presented in Chapters II through IV. The goals of the FILE-II experiment are to develop and test a cloud detector to advance the state of technology for operational remote sensing satellites. An on-board cloud detector would provide autonomous data selection to reduce the enormous volumes of data acquired, processed, and archived by existing and planned systems.

From Chapter II it has been established that the primary observables to be classified include water, bare earth, vegetation, clouds, snow, and ice. Furthermore, this separation may be performed by sampling in the four bands:

0.65 μm center, 20 nm bandwidth
0.85 μm center, 20 nm bandwidth
1.25 μm center, 150 nm bandwidth
1.55 μm center, 100 nm bandwidth

and implementing multi-spectral ratio algorithms.

Results of the IR detector survey indicate that a 128 linear germanium array is the most appropriate sensor for cameras operating in the 1.25 μm and 1.55 μm bands. It has been determined that redesign of the .65 μm and .85 μm cameras flown on FILE-I is also essential for the following reasons:

1) Integrating times are incompatible. The area arrays integrate over a complete frame, whereas the germanium linear arrays integrate over one line. This results in inadequate output level from the germanium array if it is scanned fast enough to keep up with the existing area arrays. On the other hand, if the area array scanning is slowed, dark current effects become objectionable, and image smear would be unacceptable.

2) Interlacing of lines in the area array is incompatible with the mechanically scanned linear arrays. The expense involved in providing interlace for the linear arrays or removing it from the area arrays would appear to exceed the cost of redesigning the two existing cameras.

3) Alignment of pixels with the two-scan formats is not accurate, because the linear arrays have, in effect, a cylindrical focal plane, while the area arrays have a flat focal plane. The result is that pixels in one image cannot be made to correspond to the same points on the ground if the two different scanning modes are used in the same system.

4) Alignment is simplified by using a common scanning mirror for all cameras. Using a mix of linear arrays and area arrays would require phase-locking between the rotating mirror, the linear array scanning and the area array scanning. Furthermore, all these would be a function of aircraft/spacecraft speed, complicating the electronics even more.

5) Linear arrays of about 100 elements can be compensated for gain variation and dark signal. This is not practical with a 10,000-element area array. This advantage was not considered to be enough to dictate a mechanical scanning in FILE-I because the mechanical scanning is more expensive. However, in FILE-II, the mechanical scanning is required for the IR channels, and the marginal cost of an additional channel--given that we already have the scanning implemented--is relatively small.

The currently favored camera design would use a rocking mirror driven by a ball reverser rather than a rotating mirror. This has two advantages over a rotating mirror:

1) The interval between pictures can be much shorter;

2) A ball reverser driven by a stepper motor can correct for image distortion, caused by the cylindrical focal plane, in one axis;

3) More torque is required for a cam driven scanner.

A 32^{o} square field of view appears to represent a reasonable compromise among the constraints imposed by vehicle motion, detector sensitivity, vignetting, noise and the like.

It was hoped that a Reticon CP-64 style multiplexer could be used to scan the germanium array. However, this approach has been found to be impractical due to the fact that the Reticon device requires that the photodiodes be used in a biased mode. With bias, diode dark signal would be unacceptably high. An alternate approach which is attractive employs one amplifier for each picture element. Hybrid integrated circuits, each comprising 16 transimpedance amplifiers and 16-channel analog multiplexers, would be used for scanning. Eight circuits of this type would be required. The technique is essentially the same as was used in the IR radiometer.

A tentative design for the amplifier/multiplexer hybrid circuits has been produced. In each of the two germanium cameras, the sensor will be in a two-inch square flat pack by itself. The amplifiers will be grouped, 16 per hybrid circuit, with 16:1 analog multiplexers on eight identical flat packs each approximately one-inch square. The circuit for each amplifier channel is as shown in Figure V-1.

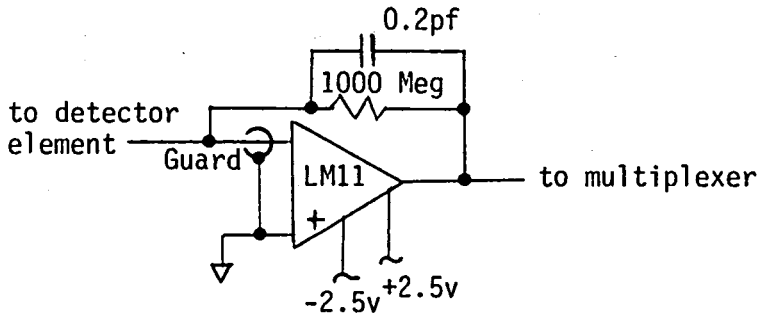

Figure V-1 Transimpedance Amplifier (16 used per package)

Two important factors recommend a hybrid circuit:

1) The part values (1000 Meg and 0.2 pf) are best achieved in hybrid form, as stray capacitance and leakage are well controlled.

2) This form of packaging allows the 128 amplifiers to be located close to the cameras. This is essential to minimize noise pickup at the low signal levels involved.

The operational amplifiers tentatively selected are LM11 integrated circuits from National Semiconductor. These devices have great advantages:

1) Very low offset voltage -- Most other devices would produce temperature-sensitive offsets superimposed on the signal with a level many times greater than the signal itself.

2) Very low power consumption -- This is important because the 128 devices are rquired to be close to the temperature-sensitive detectors due to noise-pickup considerations.

3) Acceptable noise level -- While lower-noise devices are available, the other devices do not have the offset voltage stability of the LM11 and typically use an order of magnitude more power.

Standard 55mm, F/1.4 camera lenses designed for 35mm photography, are being considered as the lenses for the germanium cameras. Inasmuch as these are mass-produced items, the use of such lenses should result in a significant cost savings over a unique optical system designed for the application. The large aperture required would otherwise require a lens design significantly more expensive than the FILE-I cameras. The lenses for the silicon cameras are expected to be simple, cemented doublets.

The VILAT processor, described in Chapter IV, was originally conceived out of necessity for the pointing and tracking phase of the FILE experiments. However, as the development effort progressed, it became apparent that significant benefits could be derived by incorporating the processor into the FILE-II design. Not only would this reduce the hardware complexity, but it would provide flexibility as well. The configuration of the FILE-II system, with the integrated processor, can be illustrated as shown in Figure V-2.

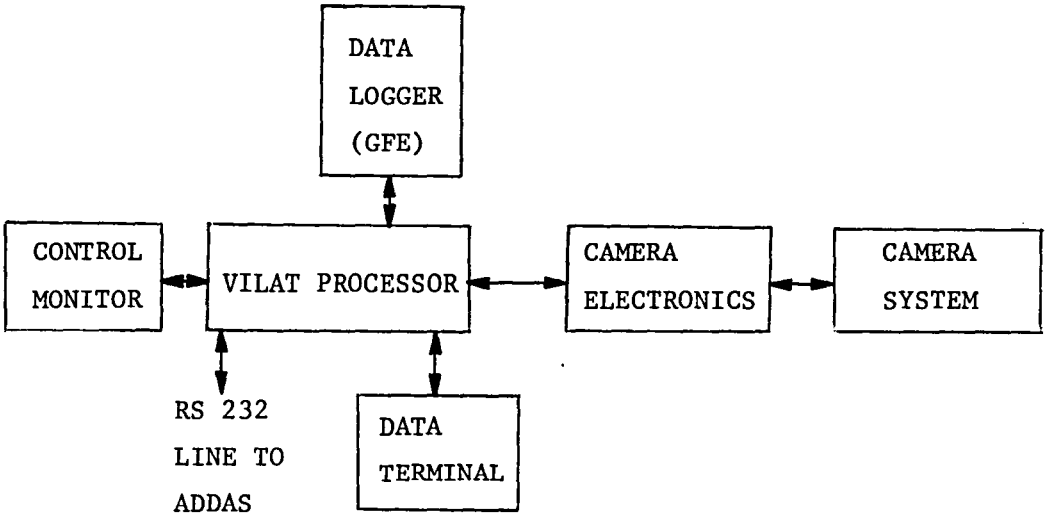

Figure V-2 FILE-II Block Diagram

The final decision required for the definition of the FILE-II experiment was whether to proceed with multiple optics as with FILE-I or single optics. A tradeoff was performed resulting in the following considerations:

1) The silicon and germanium arrays require different focal lengths. For a single optics system this would imply additional internal complexity.

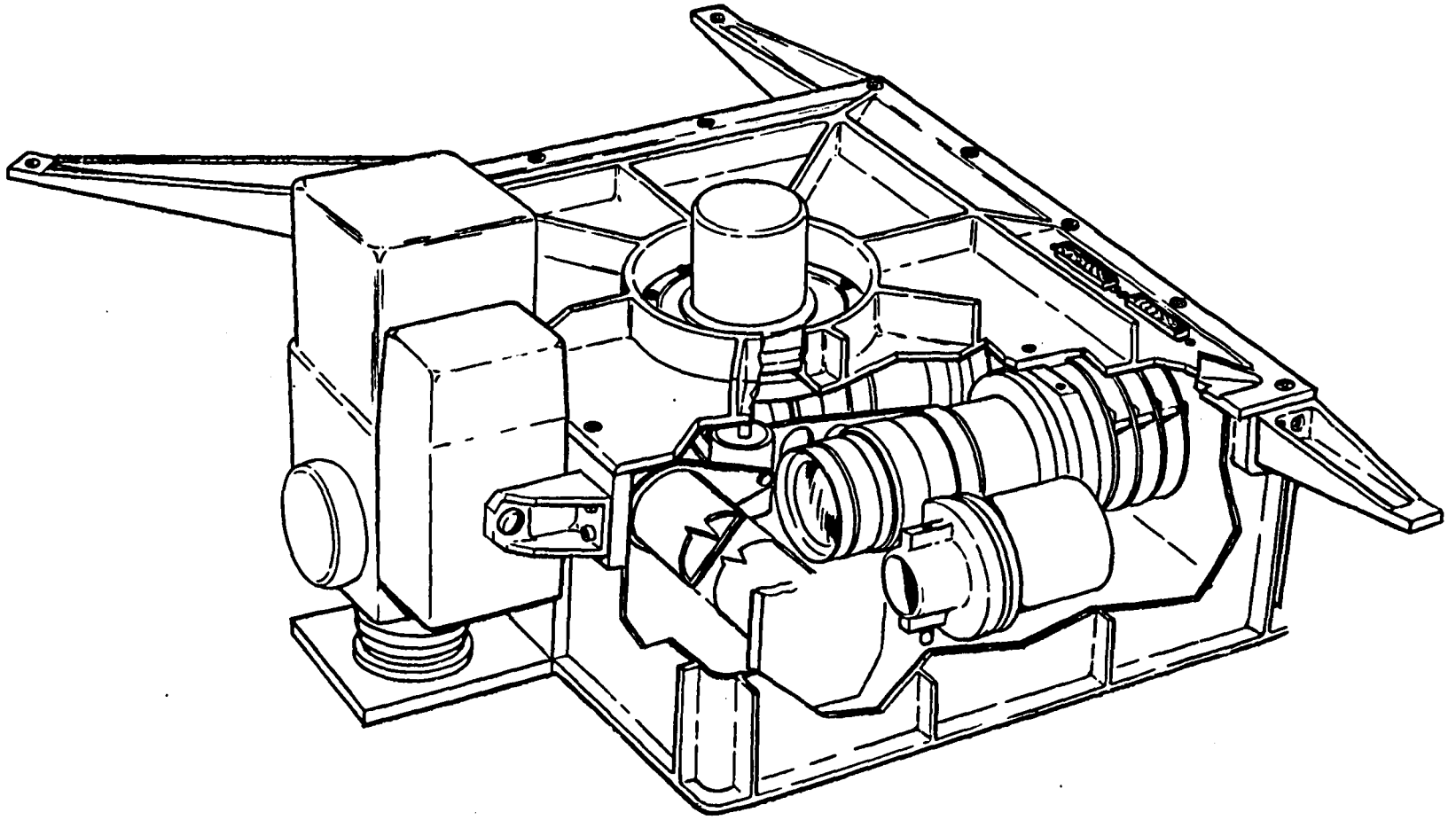

Figure V-3 Camera System

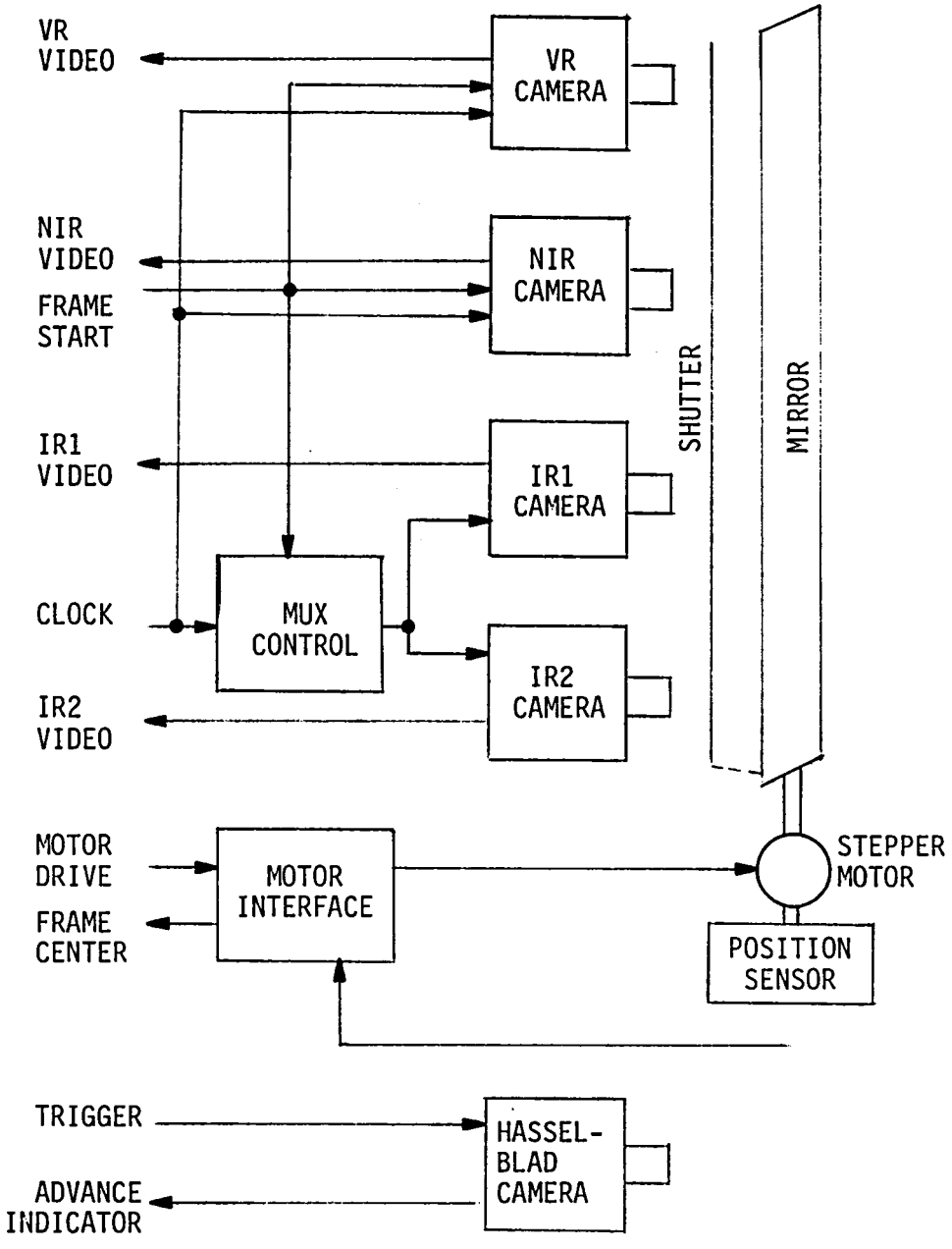

Figure V-4 Camera System Block Diagram

2) Arrays are large enough that they must be separated by more than the longest focal length. The complexity of the optics required to compensate for this factor was considered unacceptable.

3) Filters are less accessible on a single lens design.

4) The focal length of a single lens varies with wavelength. This chromatic aberration is more difficult to resolve with single optics.

5) Lens matching is not a limiting factor in registering the four images.

As a result of these factors the decision was made to design FILE-II with four sets of optics with the scan being provided by a common mirror shaft driven by a stepper motor. The preliminary camera system design is illustrated in Figure V-3 and the mechanical design is illustrated in Figure V-4.

The FILE-II preliminary design has the following basic features:

4 Cameras (20-degree field of view)

- 0.65 μm center, 20 nm bandwidth
- 0.85 μm center, 20 nm bandwidth
- 1.25 μm center, 150 nm bandwidth
- 1.55 μm cneter, 100 nm bandwidth

GFE 70mm Film Camera (36-degree field of view)

Data Logger (GFE)

- 10 megabytes storage (135 scenes)
- 7.4 kilobyte per second data rate

Control Monitor

- Operator control
- Quasi-real time display

Programmable Controller

- Data storage buffer
- Flight computer interface
- Display control
- Camera scan control
- Operator interface

The configuration of the FILE-II experiment provides flexibility to evaluate various classification algorithms, different bands, and other sensor control algorithms such as land-water tracking and correlation.

CHAPTER VI DATA ANALYSIS PROCEDURES

One of the key areas of imaging systems development which is often overlooked or incompletely performed is the post-flight data analysis. Perhaps one of the primary reasons for this is that classical approaches to the problem are extremely time consuming and so esoteric that few people are qualified to perform the analysis. This chapter describes a set of tools designed for FILE-I post-flight analysis. The tools are aimed at speeding the analysis process and simplifying the techniques so that minimum training is required.

A. DATA TRANSFER

Prior to analysis, the data from the FILE-I tape recorder must be transferred to computer compatible tape. This is accomplished by connecting the tape playback unit to a special FILE interface on the PRIME-550 (Figure VI-1) computer at the Martin Marietta Denver Aerospace Inertial Guidance Laboratory. The data and clock inputs of the interface are connected to the corresponding output of the playback unit and the playback unit power supplies turned on.

To copy the data, a computer tape is mounted on the tape drive and advanced to the load point. The drive is then placed "on line" and the program "FTFLE" run under the PRIMOS-II operating system.

Program "FTFLE" writes raw data onto the tape but, due to timing constraints, does not reformat the data for ease of use. The resulting format is illustrated in Table VI-1. A reformatting program is then executed to remove scan interlace, decode time-word and pixel-count information, add frame count and title information, and delete the unused words that the buffer memory appends to each record. The reformatting program, named "*REFRM", reads the tape onto disk and then rewrites the reformatted data onto the same tape or another tape. The tape from this operation is then used as input to the data analysis programs.

B. DATA ANALYSIS

Analysis of multi-spectral classification techniques must be performed on two levels. A micro-scale analysis which concentrates on individual scenes is required to identify specific misclassification problems, whereas macro-scale analysis operating on the statistics for the population of all scenes is required to insure that the algorithm performs well over a wide variety of conditions. Without either of these techniques, the analysis would produce limited results and may eventually lead to erroneous conclusions. For this reason, the multi-spectral data analysis programs were functionally separated as shown in Figure VI-2 and combined into a single package.

1. Micro-Scale Analysis -- Micro-scale analysis of multi-spectral data is an interactive process resulting in the optimization of the classification algorithm for a single scene. After sequential analysis of each scene is performed, the results are combined under macro-analysis to establish the optimum algorithm for the broader population.

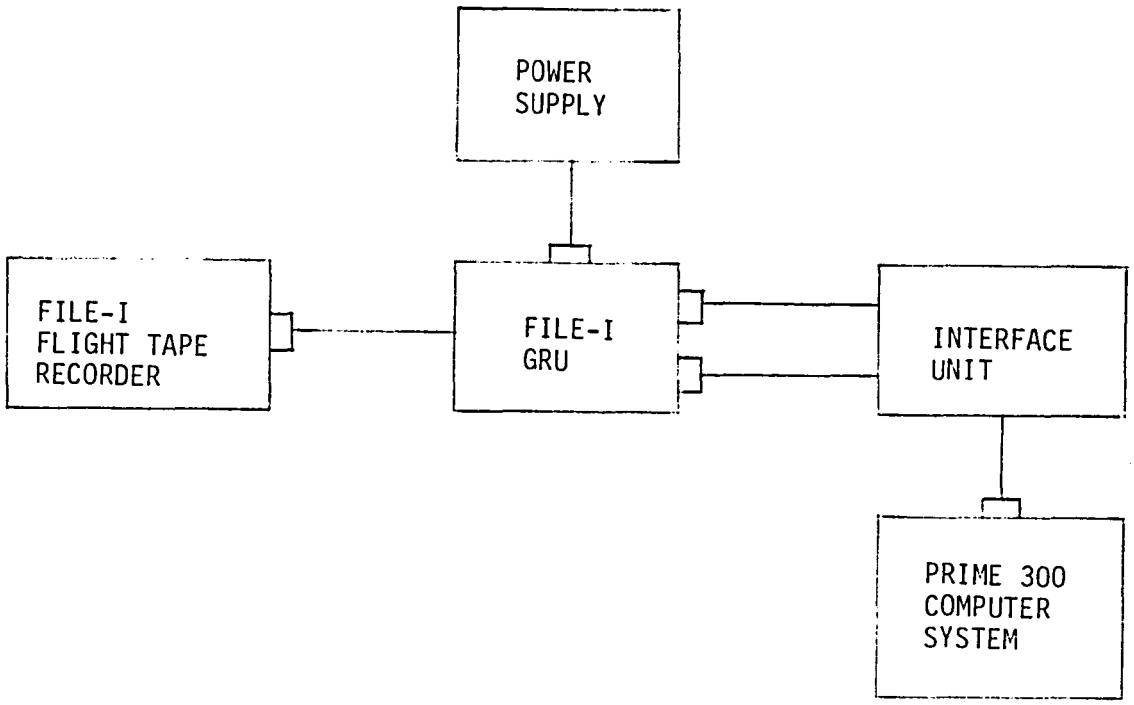

Figure VI-1 Data Transfer Block Diagram

Table VI-1 9-Track Mag Tape Format

THE TAPE FORMAT IS AS FOLLOWS -

BLOCK 1
ID BLOCK
ONE (1) RECORD

EOF MARK

DATA BLOCK 1
PICTURE #1

51 RECORDS

EOF MARK

DATA BLOCK 2
PICTURE #2

51 RECORDS

EOF MARK

DATA BLOCK N
PICTURE #N

51 RECORDS

EOF MARK

EOF MARK

THE ID BLOCK FORMAT IS:

WORD	DESCRIPTION
1-36	TITLE (2 ADCII CHARACTERS/WORD)
37	NUMBER OF FRAMES ON FLIGHT TAPE
38	NUMBER OF PROCESSED FRAMES ON THIS
39	FRAME 1 DAY
40	FRAME 1 HOUR
41	FRAME 1 MINUTES
42	FRAME 1 SECONDS
43	FRAME 1 IDENTIFIER
44	LAST FRAME DAY
45	LAST FRAME HOURS
46	LAST FRAME MINUTES
47	LAST FRAME SECONDS
48	LAST FRAME IDENTIFIER
49-400	ZERO

THE DATA BLOCK RECORD FORMAT IS
RECORD 1 (ID RECORD)

WORD	DESCRIPTION
1	FRAME NUMBER (FROM ORIGINAL FLIGHT)
2	DAY
3	HOURS
4	MINUTES
5	SECONDS
6	FLT CODE
7	VEGETATION PIXEL COUNT
8	WATER PIXEL COUNT
9	CLOUD PIXEL COUNT
10	BARE LAND PIXEL COUNT
11-400	ZERO

THE DATA FORMAT FOR RECORDS 2-51 IS

WORD	DESCRIPTION
1	IRA(1)
2	VRA(1)
3	IRA(2)
4	VRA(2)
399	IRA(200)
400	VRA(200)

[DATA FOR 2 SCAN LINES PER RECORD]

ALL FRAME DATA RECORDS FOLLOW THIS FORMAT

RECORD 3 CONTAINS SCAN LINES 3 & 4
RECORD 4 CONTAINS SCAN LINES 5 & 6
RECORD 5 CONTAINS SCAN LINES 7 & 8
ETC THROUGH
RECORD 51 CONTAINS SCAN LINES 99 & 100
ALL DATA IS DE-INTERPLACED SO THAT IT IS
CONTAINED ON THE TAPE IN THE RIGHT SEQUENCE
FOR FORMING THE PICTURE

A DOUBLE EOF MARK INDICATES THE END
OF THE DATA ON THE TAPE

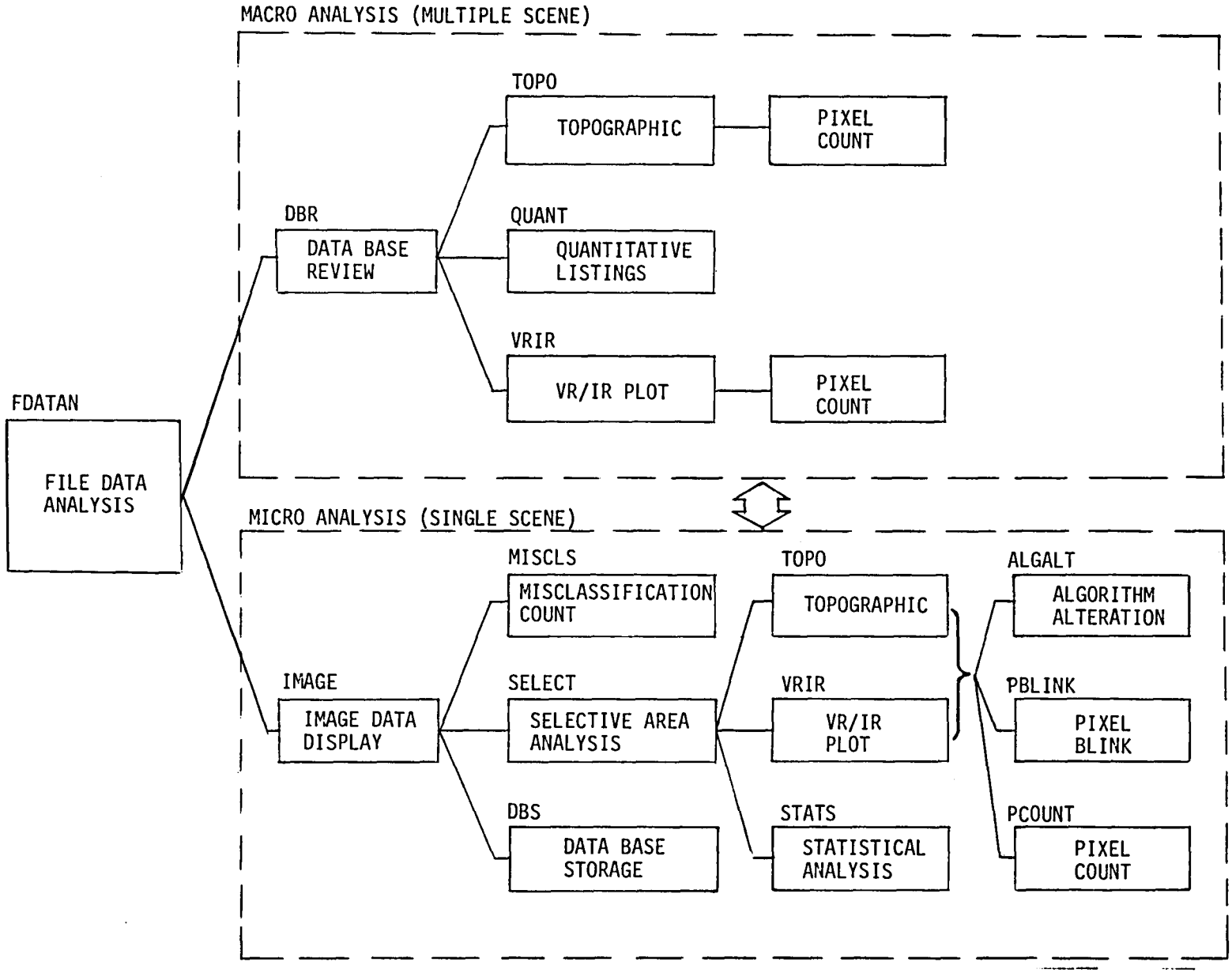

Figure VI-2 File Data Analysis Package -- Functional Block Diagram

The first step in the interactive procedure is to compare a color representation of the classified scene with a relatively high resolution color photograph of the same area to identify areas of misclassification. This comparison is easily performed with the assistance of a zoom transfer scope which allows simultaneous projections of two images with different resolutions, orientations, and perspectives. Identification of the misclassified regions will be used to establish the percentage of misclassification for each algorithm and to allow the operator to make radiometric measurements of these areas with the aid of the program.

The remainder of the analysis utilizes a computer program which has been incorporated to speed and enhance the process. The primary function of the micro-scale analysis is to display all experimental data and a multi-spectral radiance plot (Figure VI-3) of individual scenes selected by the operator. The data displayed consist of imagery from each band of the instrument, a color representation of the classified scene, and quantitative data including date of exposure, algorithm settings used, and classification counts obtained form the flight instrument, and computer model. The multi-spectral radiance plot is obtained by plotting two radiance values against one another for each pixel in the scene (Figure VI-4).

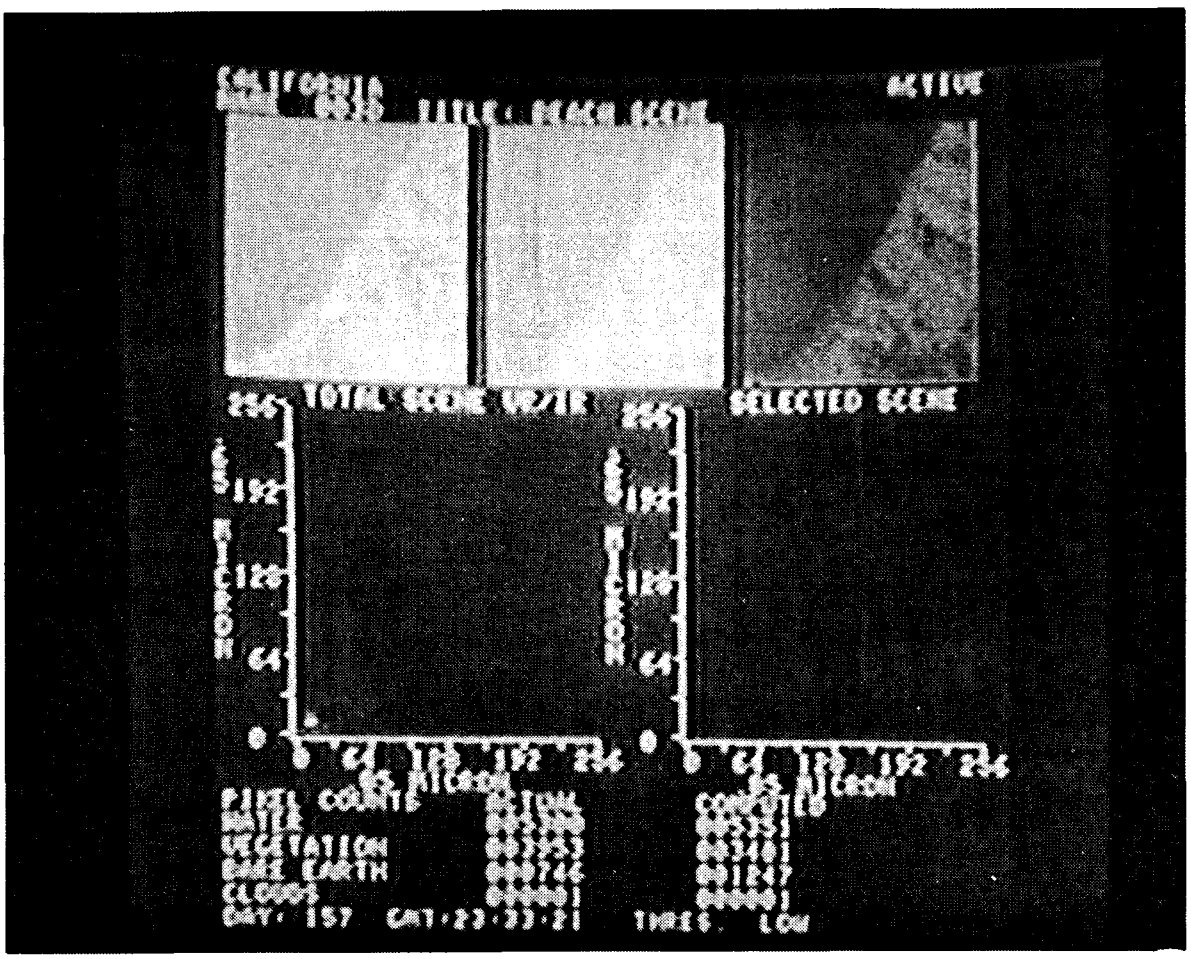

Figure VI-3 Flight Data Display Format

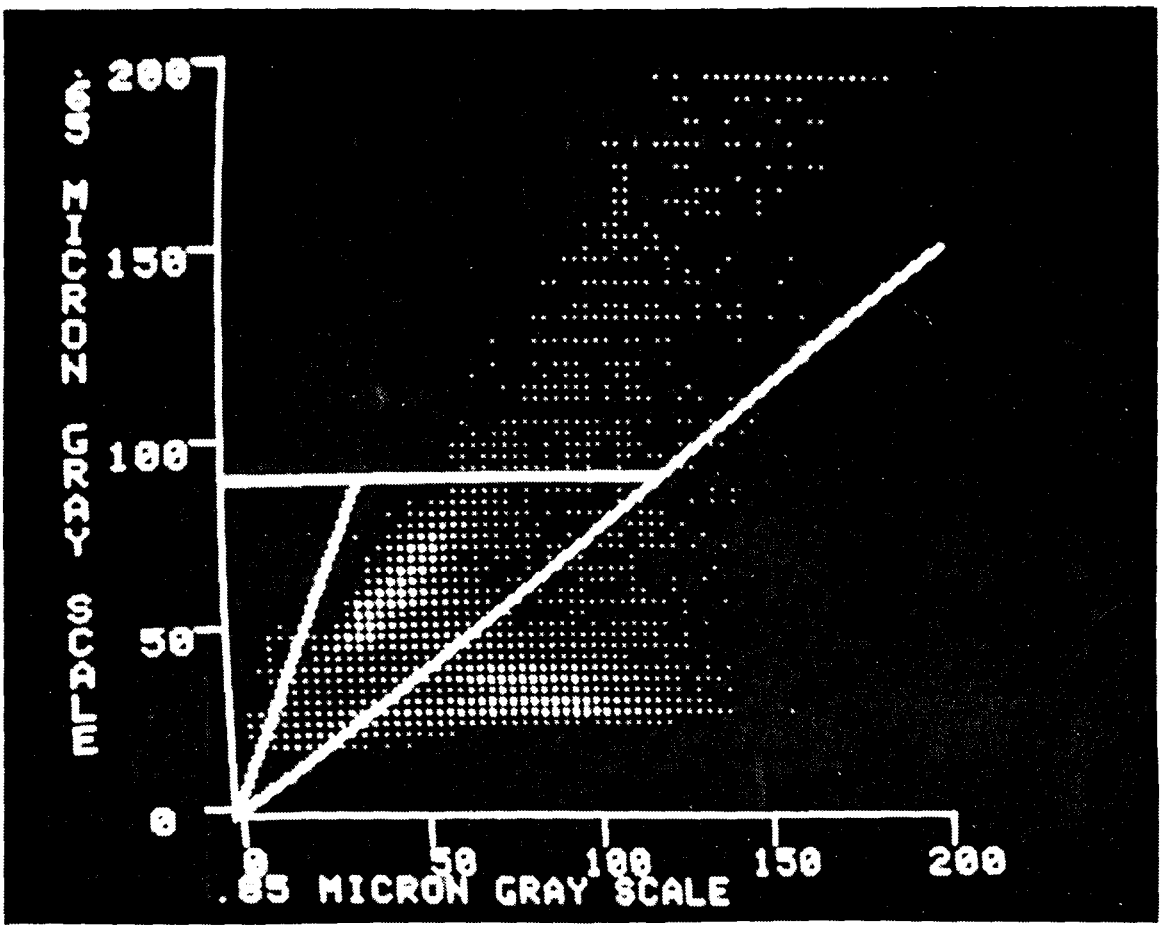

Figure VI-4 Multispectral Radiance Plot

If more than one pixel falls at a given location on the plot, the display intensity at that location is increased proportionally. This graphical representation of the radiance data allows detailed analysis of the classification algorithm through careful examination of the clusters. However, due to the large number of pixels inherent in the scene, it is difficult to understand the relationship between specific areas of the imagery and points on the radiance plot. Therefore, a special tool has been implemented which allows selected areas of the image to be identified by using an input from a joystick. A separate multi-spectral radiance plot of this data is then created (Figure VI-5). One of the primary uses of this tool is to select those areas of the scene which were misclassified and analyze the plot to understand the cause. It is also desirable to obtain radiance measurements of well defined homogeneous areas within a scene. To further enhance the tool, an additional transformation has been incorporated which allows pixels in the radiance plot

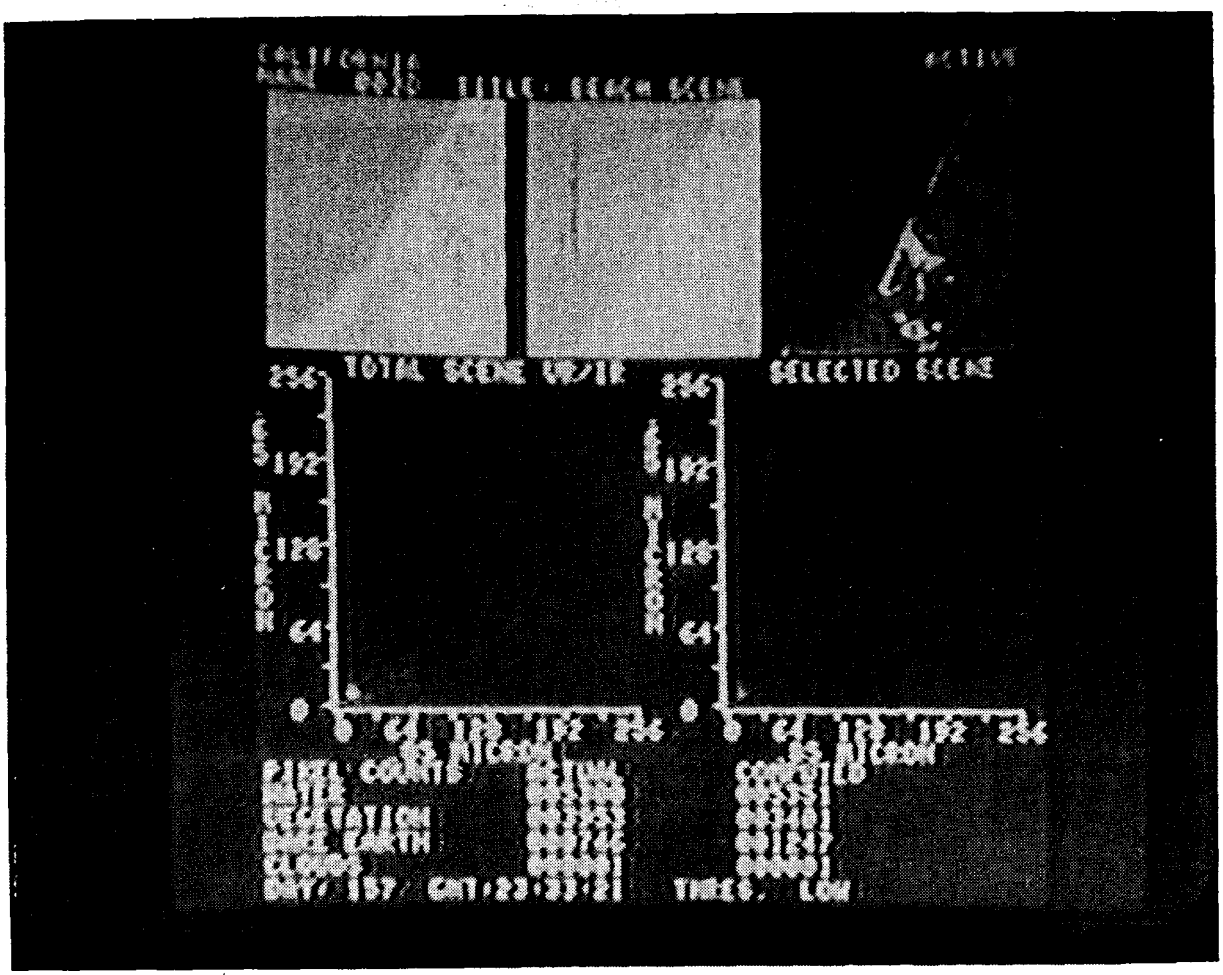

Figure VI-5 Selection of Subareas within Scene

to be selected and the corresponding imagery blinked on and off (Figures VI-6 and VI-7). These two tools have been found to be the most important features of the program because they allow an operator to gain a quick understanding of the algorithm's performance based on radiance measurements.

In the tools previously described, the primary emphasis was placed on qualitative approach to analysis relying on the image interpretation capabilities of the operator. An equally important area is a statistical analysis of the multi-spectral data in order to measure the clustering. Two types of statistical analysis have been incorporated into the program. The first approach was designed around the FILE-I multi-spectral ratio algorithm, whereas the second applies a more general approach to cluster analysis.

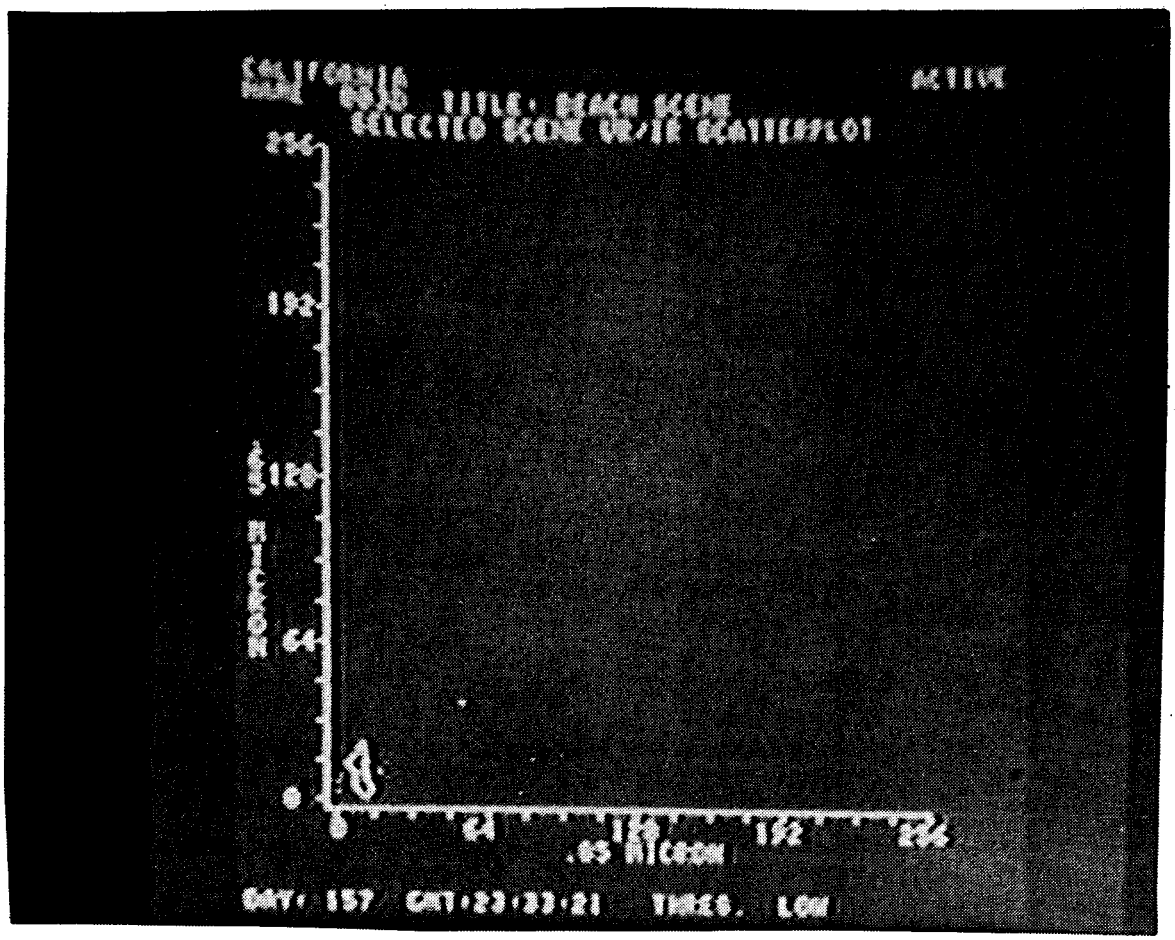

Figure VI-6 Multispectral Radiance Plot of Selected Areas and Identification of Radiance Points To Be Blinked

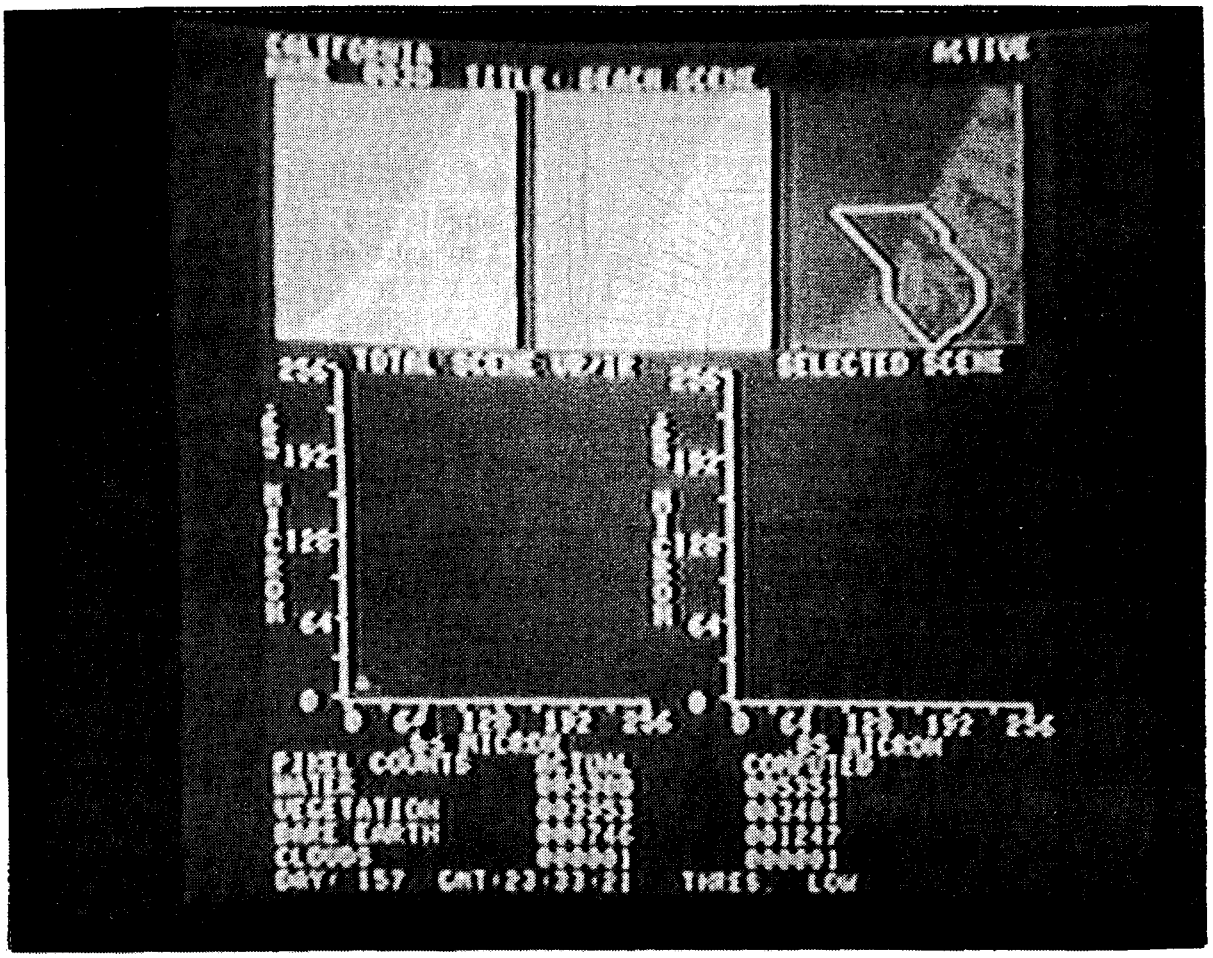

Figure VI-7 Corresponding Imagery Being Blinked

Method 1. Pixels in the multi-spectral ratio plane, which plots two spectral radiances against each other, may be converted from cartesian coordinates to polar coordinates (Figure VI-8.). The entire plane is then scanned by using equal area radial slices, and the population in each slice is counted. The resulting data are plotted in two ways. The first plots the population as a function of angular component, and the second plots the population as a function of radial component (Figure VI-9). Ideally, for the FILE-I algorithm, it is desirable to obtain a bell-shaped histogram where the peak is centered

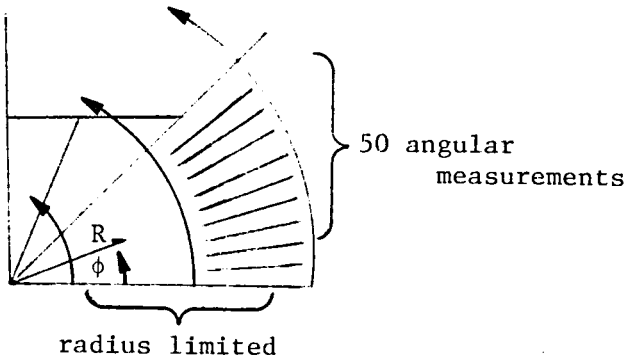

Figure VI-8 Transformation of Multispectral Radiance Plane from Cartesian Coordinates to Polar Coordinates

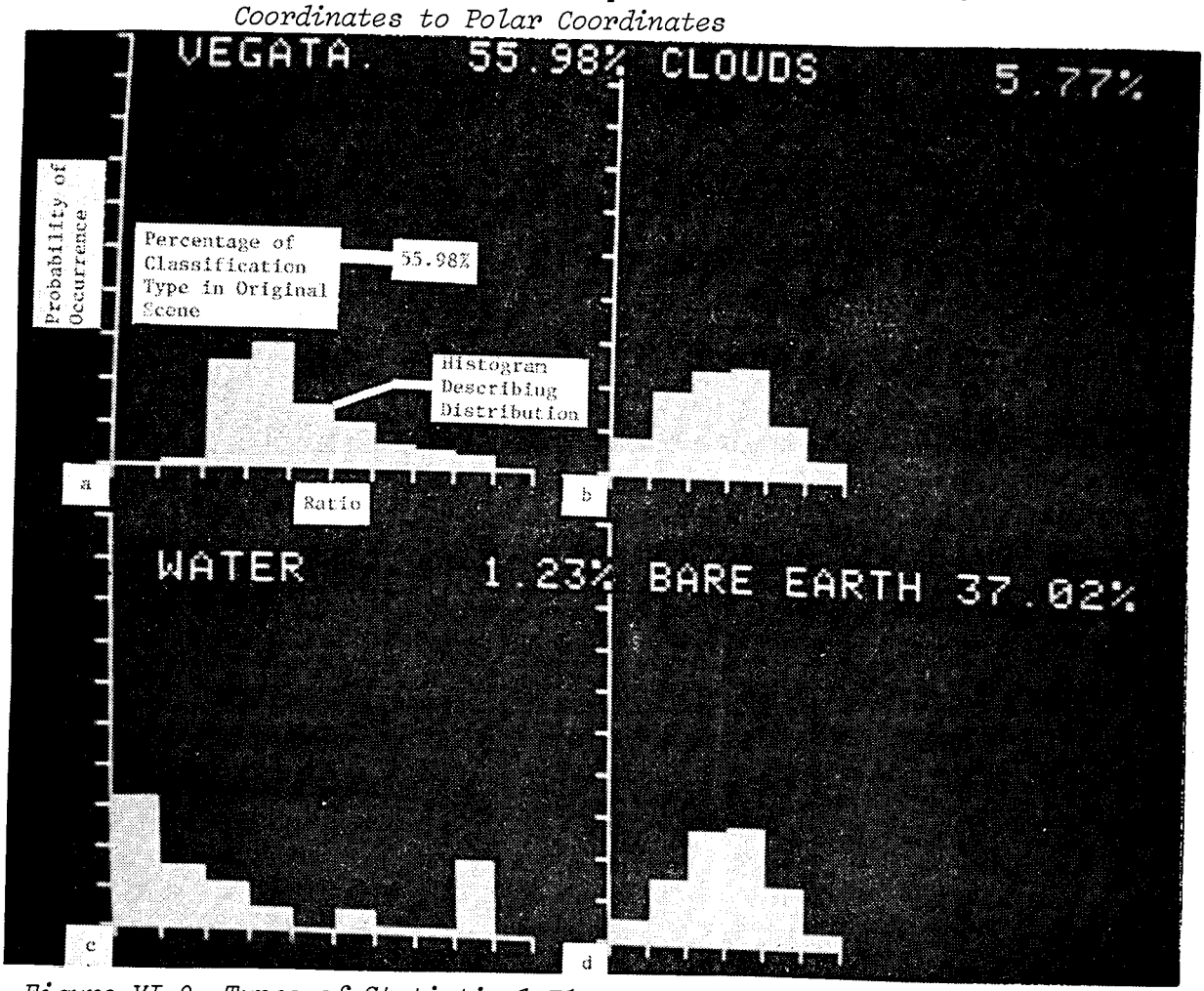

Figure VI-9 Types of Statistical Plots

in the ratio band (Figure VI-9b). This would imply an optimally selected classification boundary. However, using actual data we find distributions similar to Figure VI-9c, where pixels have clustered on or near a classification boundary. Bimodal distributions might suggest that additional features may be classified.

Method 2. While the first method has been found to be quite useful in analyzing the FILE-I algorithm, it does not provide an adequate description of the clusters themselves. For this process it was necessary to implement a more classical approach to cluster analysis. The primary observables for this analysis are:

a) the centroid of the cluster;

b) the orientation of the cluster with respect to the radiance axes;

c) the two-dimensional distribution of points relative to an axis passing through the centroid of the cluster with an orientation determined by (b).

The information gathered from the qualitive image interpretation and the quantitative statistical analysis can be combined to form a basis on which to modify the classification algorithm. A capability has been incorporated into the program which allows an operator to specify any piecewise linear classification structure. The program internally creates a classification array which has a dimension equal to the dynamic ranges of the two digital sensor outputs. For example, if one sensor quanitizes its output to 265 levels and a second quanitizes to 64 levels, the array would be dimensional as 256 x 64. Each element of the array contains a number corresponding to the classification to be made at that position in the multi-spectral radiance plane (Figure VI-10). The program then classifies the scene by using the two spectral signatures as indices into the classification array (Figure VI-11).

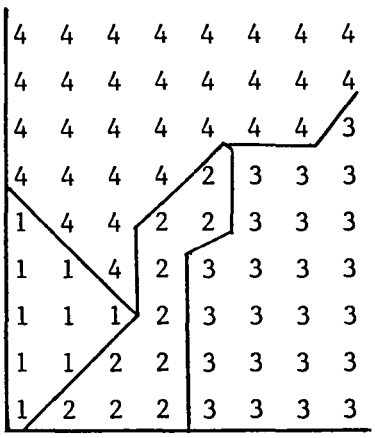

Figure VI-10 Classification Array for Two Bands with 8-Level Output

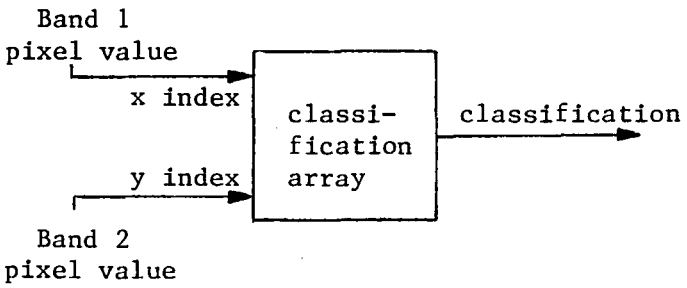

Figure VI-11 Scene Classification

2. Macro-Scale Analysis - Macro-scale analysis is intended to provide the operator with a means of predicting the performance of an algorithm, optimized for a single scene, over a larger population of scenes. Furthermore, it has been imbedded in the actual procedure, as discussed later, and has been implemented as an option in the program.

The macro analysis option creates a composite multi-spectral radiance plot of a number of scenes stored in the data base. The operator is given the capability of selecting the scenes from which the plot is to be created. In this way, the statistical nature of a single scene can be compared with that of another set of scenes in order to establish whether or not the data are representative of the broad population of imagery acquired.

Macro-scale analysis is especially important to avoid the selection of an algorithm which is only valid over a subset of the scenes acquired.

3. Multispectral Data Analysis Procedure - Up to this point the discussion has focused on the analytical tools which have been implemented in a computer program. In addition to the tools, it is vital to have a well-defined procedure in order to avoid the many pitfalls which add to the complexity and the time of analysis. Figure VI-12 illustrates the procedure around which the multi-spectral data analysis programs were developed.

The process begins by examining the data and editing out the scenes for which the experiment was not designed. For example, the optics on FILE-I were designed for a sun angle greater than 40^{o}. If data are gathered with lower sun elevation, they are edited out of the analysis. In this way, excessive amounts of time are not spent on the analysis of useless data. The remainder of Figure VI-12 illustrates how the analysis tools are used in the reduction of the FILE-I data.

By combining the procedural definition with the analysis program design, it is possible to direct the analysis along a well-defined path, thus reducing the time involved. However, it is important to incorporate enough flexibility into the procedure so that the operator is not unintentionally limited.

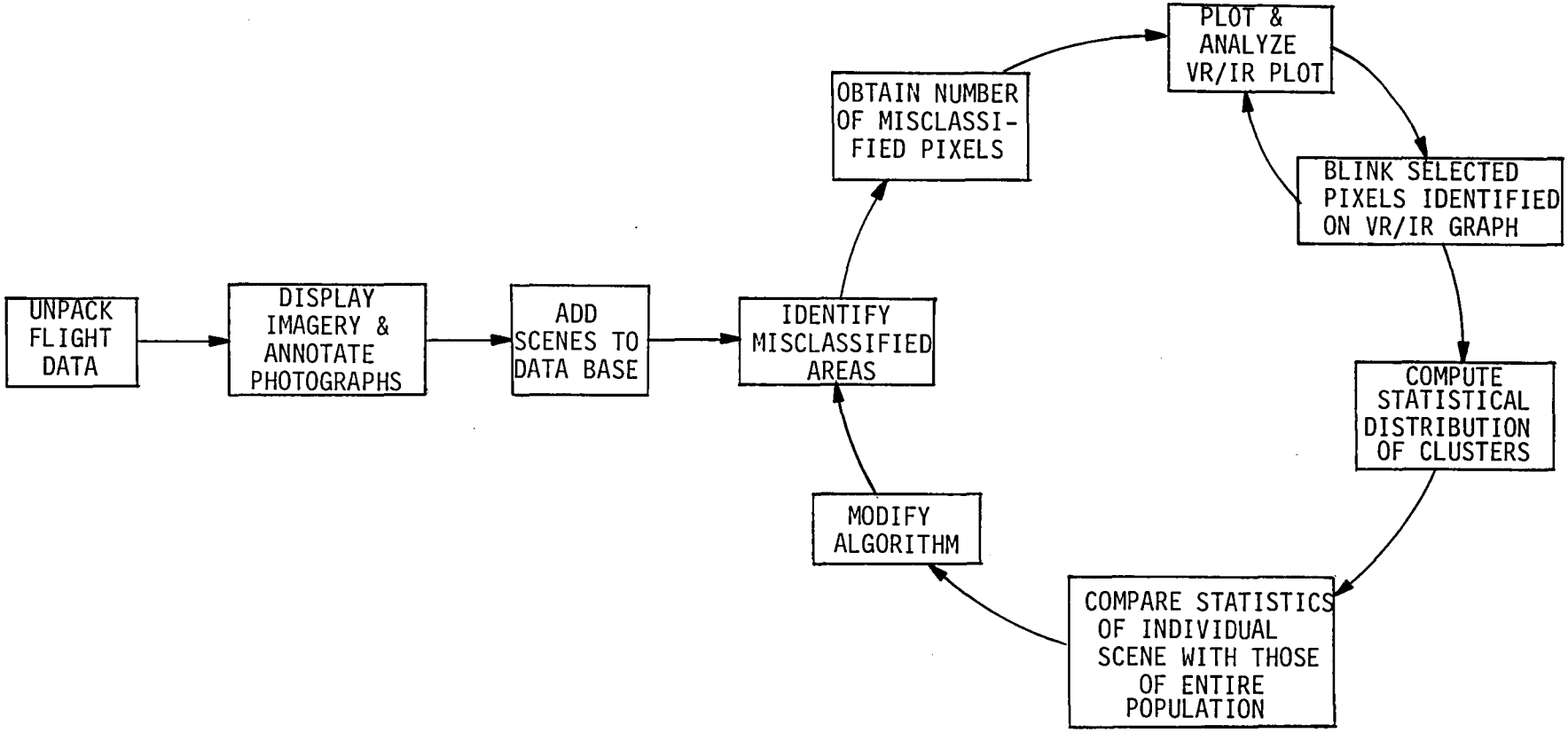

Figure VI-12. FILE Data Analysis Procedures

CONCLUDING REMARKS

More complete data analysis techniques and procedures were developed for use in working with FILE digital and photographic data. Included were methods to reformat the flight data onto computer compatible tapes; to display imagery and annotate photographs; to identify and analyze misclassified areas; to display data clusters and compute their statistical distributions; to compare statistics of an individual scene with those of the entire population (data from flight); and to modify and optimize the classification algorithm.

A number of ground investigations were performed to provide the basis for designing a more advanced version (four-band) of the FILE, which would be capable of classifying clouds and snow (and possibly ice) as distinct features. The original FILE design (two-band) provided for classifying water, bare land, vegetation, and clouds/snow/ice (grouped). The more advanced FILE (FILE II) design would have the classification capabilities of the two-band instrument plus the more advanced capabilities.

The investigations included the development of a sensor system design and field measurements to test it. The sensor system was based on 128-element silicon CCD linear arrays for the 0.65 μm and 0.85 μm spectral bands, and 128-element germanium linear arrays, coupled with hybrid integrated circuits, for bands at 1.25 μm and 1.55 μm. Tradeoff studies led to the choice of these bands and an instrument design that included four separate cameras. The instrument was designed to provide a 128- x 128-pixel image format via scanning mirrors (on a common rotating shaft) to scan the detector arrays across the field of view.

In the implementation of the two-band FILE algorithm, the control and classification logic was not complex enough to require a general-purpose processor. However, the FILE II, with four spectral channels, requires greater processing flexibility. As a means to accommodate FILE II, and also to provide a data processing base for addressing questions in landmark recognition and tracking and instrument pointing applications, a digital signal processor was designed and built. The processor was eventually incorporated into FILE II.

1. Report No.	2. Government Accession No.	3. Recipient's Catalog No.
NASA CR-166066		

4. Title and Subtitle	5. Report Date
Study and Simulation Results for Video Landmark Acquisition and Tracking Technology (VILAT II)	February 1983
	6. Performing Organization Code

7. Author(s)	8. Performing Organization Report No.
J. W. Lowrie, J. C. Tietz, H. M. Thomas, K. D. Gremban, C. Hughes, and C. Y. Chang	
	10. Work Unit No.

9. Performing Organization Name and Address	11. Contract or Grant No.
Martin Marietta Aerospace, Denver Division Post Office Box 179 Denver, CO 80201	NAS1-15602
	13. Type of Report and Period Covered
12. Sponsoring Agency Name and Address	Contractor Report
National Aeronautics and Space Administration Washington, DC 20546	14. Sponsoring Agency Code 506-61-03

15. Supplementary Notes

Langley technical monitor: R. Gale Wilson
Final Report

16. Abstract

The results of several investigations and hardware developments are described which supported new technology for Earth feature recognition and classification. Data analysis techniques and procedures were developed for processing the Feature Identification and Location Experiment (FILE) data. This experiment was flown in November, 1981, on the second Shuttle flight and a second instrument, designed for aircraft flights, was flown over the United States in 1981. Ground tests were performed to provide the basis for designing a more advanced version (four spectral bands) of the FILE which would be capable of classifying clouds and snow (and possibly ice) as distinct features, in addition to the features classified in the Shuttle experiment (two spectral bands). The Shuttle instrument classifies water, bare land, vegetation, and clouds/snow/ice (grouped).

17. Key Words (Suggested by Author(s))	18. Distribution Statement
feature classification landmark tracking spectral ratioing Shuttle experiments	Unclassified - Unlimited Subject Category 43

19. Security Classif. (of this report)	20. Security Classif. (of this page)	21. No. of Pages	22. Price
Unclassified	Unclassified	79	A05

For sale by the National Technical Information Service, Springfield, Virginia 22161

End of Document